



Review article

Hydrothermal synthesis of nano-metal oxides for structural modification: A review



Tasnimul Quader Tazim ^b, Md. Kawsar ^{a,b}, Md. Sahadat Hossain ^{a,*},
Newaz Mohammed Bahadur ^b, Samina Ahmed ^{a,*}

^a Glass Research Division, Institute of Glass & Ceramic Research and Testing, Bangladesh Council of Scientific and Industrial Research (BCSIR), Dhaka 1205, Bangladesh

^b Department of Applied Chemistry and Chemical Engineering, Noakhali Science and Technology University, Noakhali, Bangladesh

ARTICLE INFO

Keywords:
Nanomaterials
Hydrothermal
Synthesis
Metal oxides

ABSTRACT

Materials with a minimum of one dimension less than 100 nanometers (nm) are referred to as nanomaterials (NMs), granting them unique and intriguing properties due to their minimal size. NMs exhibit unique thermal, magnetic, optical, and chemical properties that distinguish them significantly from larger molecules such as micromolecular, bulk organic, or inorganic compounds. Metal oxide NMs are utilized in the medical sector for targeted drug delivery, environmental science for pollution management and water treatment, and electronics to improve energy production. Because of the rapidly growing demand for nanomaterials with precise morphological properties for specific applications, significant research efforts have been directed toward developing hydrothermal synthetic methodologies under various reaction conditions to achieve both scientifically and practically novel results. Several studies have been conducted to study the impact of various response parameters on the fundamental characteristics and morphology of MNs. Therefore, this review paper discussed the hydrothermal synthesis under different reaction conditions for seven important metal oxides (ZnO , CuO , Fe_2O_3 , CdO , TiO_2 , Al_2O_3 , and CaO). Furthermore, it analyzes how utilizing varied source materials alongside diverse reaction parameters affects the structural morphology of these nanoscale materials, facilitating their development for specific applications.

1. Introduction

Nanomaterials (NMs) are characterized by having a minimum of one dimension (height, width, length) that is less than 100 nanometers (nm) [1]. Their minimum dimensions give them specific chemical and physical properties. These NMs may be categorized into structures having 0D, 1D, 2D, or 3D [2]. They may be formed in single or multiple layers and have either a crystalline or amorphous structure [3]. The categories included in this category consist of a diverse range, including thin films, nanoplates, and nanocoating. Additionally, NMs incorporate multiple nanocrystals in diverse orientations, such as nanotubes, carbon nanobuds, fibers, foams, pillars, polycrystals, fullerenes, and layered skeletons [4].

Nanoparticles (NPs) are used in several industries, such as petrochemicals, water treatment, building materials, industrial and catalytic processes, diagnostics, and medicine delivery [5]. Metal oxide nanoparticles have unique thermal, magnetic, optical, and chemical

characteristics compared to their bulk counterparts. These unique properties have resulted in widespread application in a range of sectors, including medicine, catalysis, and electronics [6]. The performance of such nanoparticles strongly depends significantly on factors such as particle structure, dimension, and morphology, among others. Several synthesis methods were utilized to synthesize NPs, such as the chemical vapor deposition method [7], solvothermal method [8], microemulsion method [9], wet precipitation method [10], thermal decomposition technique [11], sol-gel method [12], and hydrothermal method [13]. Hydrothermal is environmentally favorable among these various synthesis methods, converting aqueous metal salt solutions into metal oxides. It utilizes water as a solvent, reducing the need for hazardous organic solvents, and operates under milder conditions than methods requiring high temperatures or toxic reagents [14]. This method creates a high-temperature and pressure reaction environment by using an aqueous solution inside a specially designed sealed reaction vessel (Fig. 1) by heating and pressurizing the reaction system [15]. This

* Corresponding authors.

E-mail addresses: saz8455@gmail.com (Md. Sahadat Hossain), shanta_samina@yahoo.com (S. Ahmed).

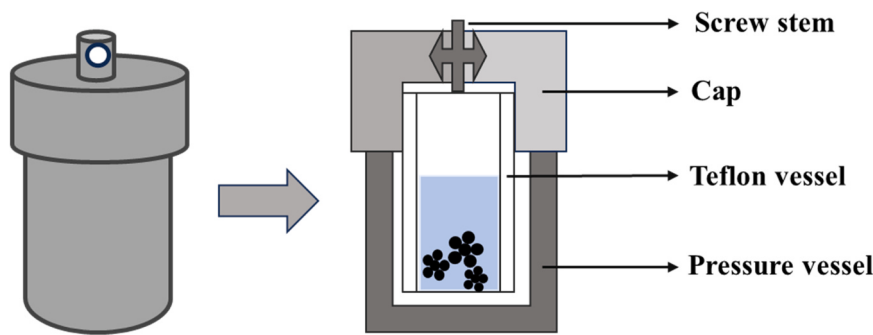


Fig. 1. Diagram of standard equipment used for the hydrothermal method.

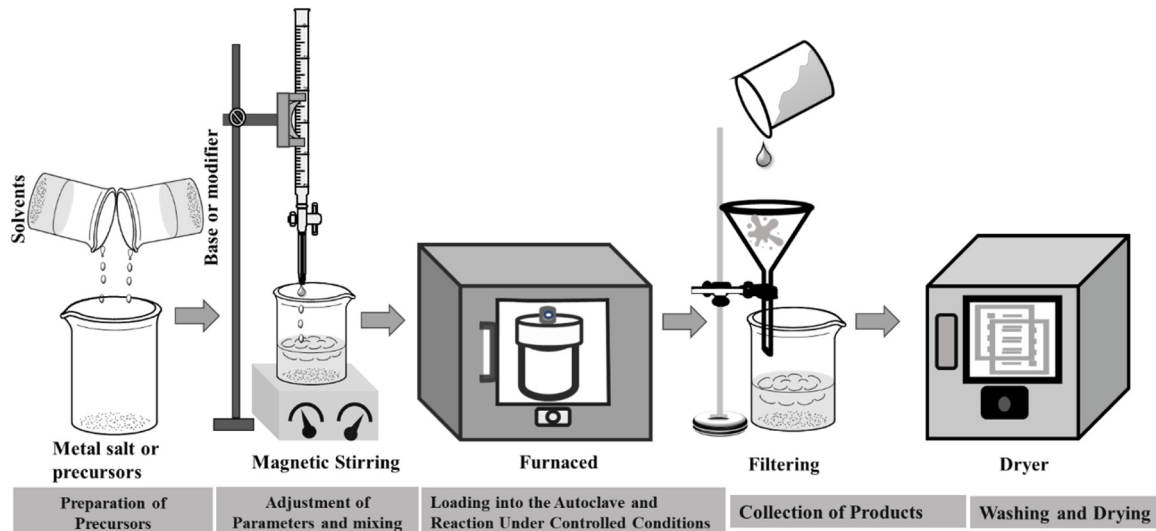


Fig. 2. Schematic representation of the hydrothermal nano metal oxide synthesis.

method offers precise nanoparticle size, shape, and morphology control, promotes highly crystalline products, and minimizes impurities by reducing contamination and secondary reactions. It is versatile, suitable for synthesizing metal oxides and composites, easily scalable for industrial applications, and suitable for crystal structure modification with the help of organic modifiers [16].

Hydrothermal synthesis involves synthesizing crystalline materials by subjecting a sealed solution to moderate temperatures and pressures by accelerating chemical reactions (Fig. 2). This method uniquely enables NPs to synthesize through the condensation and hydrolysis process of metal salts within the reactive solution [17]. In this way, the structure, morphology, and size of the synthesized NPs may be precisely regulated. Additionally, the chemical and physical characteristics of the resultant oxides can be controlled by modifying reaction parameters, including temperature, pressure, pH, solvent composition, additives, and precursor concentration [18]. Such control is essential because there is a direct relationship between these attributes and the oxides' appropriateness for specific applications. Temperature (100–500 °C), reaction time, and pressure must be controlled to keep the solvent liquid. Water is commonly used as the solvent; other solvents may be employed to customize different aspects of crystals. Reaction time significantly influences the crystal's specific shape formation and controlled dimensions. Solution pH, reactant concentration, and additives significantly affect crystal formation and morphology, and pH can be adjusted across a broad spectrum, from acidic ($\text{pH} < 2$) to alkaline conditions ($\text{pH} > 10$). Surfactants selectively adsorb onto specific crystal planes, controlling their growth rates and shaping the material. They stabilize nucleation, prevent particle aggregation, reduce surface energy, and act

as templates for organized self-assembly, ensuring uniformity and size control [19].

Among all nanoparticles, some metal oxides NMs such as ZnO, CuO, Fe₂O₃, CdO, TiO₂, Al₂O₃, and CaO are prominent nanoparticles with a wide range of applications in energy generation, electronics, environmental remediation, and other industries because of their unique properties. ZnO and TiO₂, characterized by high refractive indices and semiconductor properties, are frequently utilized in gas sensors, photocatalysts, dye-sensitized solar cells, and sunscreens [20]. TiO₂ is also used increasingly in biological applications, renewable energy, and pollutant degradation [21]. Fe₂O₃ is known for its magnetic properties and is employed in catalysts, purification, biomedical, gas sensors, electronics, and pigment [22]. CuO is widely used in gas sensors as a sensing material [23]. CaO is required in cement manufacturing and the desulfurization process in steel production. CdO and CuO exhibit high transparency and conductivity, making them suitable for photocatalysis, gas sensors, transistors, solar cells, and photovoltaic applications [24, 25]. Al₂O₃ is a commonly used ceramic material due to its exceptional heat resistance, mechanical strength, wear resistance, hardness, low electrical conductivity, and robust corrosion resistance in various chemical conditions. It is also used in catalysts, supporters of catalysts, and absorbents [26, 27]. The hydrothermal synthesis method offers distinctive benefits for synthesizing such oxides because it leads to well-defined and pure crystalline phase formation, which is necessary for improving their efficiencies in some applications [28].

This review paper aims to evaluate the hydrothermal synthesis method of metal oxides, with special emphasis on the different mechanistic pathways and how synthesis parameters affect the properties and

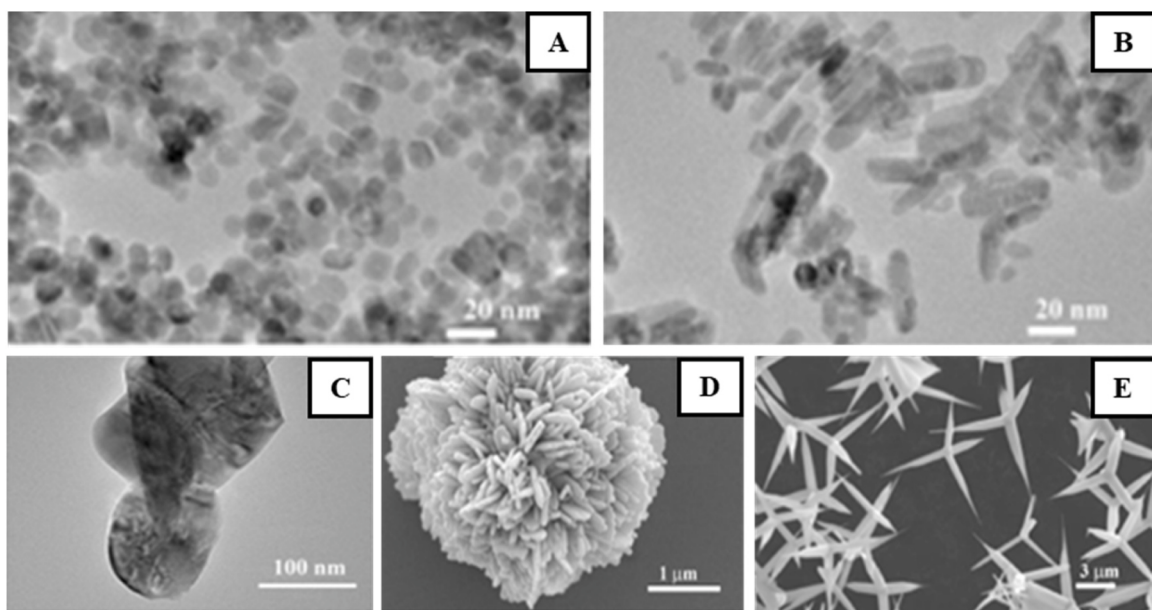


Fig. 3. TEM and SEM images of ZnO nanoparticles and microparticles: (A) nanoparticles, (B) nanorods, (C) particles, (D) hierarchical structures, (E) tetrapods [38].

morphology of the NMs. To achieve this goal, a comprehensive review and experimental analysis have been conducted to demonstrate the advancements achieved in hydrothermally synthesized oxide metal nanoparticles. This review also highlights the potential for future research and improvements in metal oxide production, inspiring further exploration and innovation.

1.1. Hydrothermal synthesis of ZnO

Nanocrystalline zinc materials and their derivatives can be synthesized using the hydrothermal synthesis method, which is solution-based. This solution-based process involves high-temperature reactions within a sealed environment [29,30]. ZnO is one of the most studied semiconductors and has significant potential for optoelectronic nanodevices. ZnO exhibits remarkable mechanical and thermal stability, a broad bandgap between 3.2 and 3.4 eV, a significant exciton binding energy of 60 meV, and an easy growing procedure [31]. The hydrothermal synthesis method is highly regarded for its capability to precisely regulate the resultant's shape, diameter, and nanostructure morphology. Various crystal structures of ZnO, such as nanobelts, nanowires, nanorods, nanobridges, nano-nails, and whiskers, have been successfully synthesized by adjusting reaction parameters (e.g., temperature, reaction time, precursor concentration, additives, and pH of the solution) [32]. While excessively high temperatures are detrimental, and low temperatures (below 80 °C) fail to synthesize the desired crystal volume and size. So, it is imperative to optimize the solution temperature to achieve the desired characteristics in ZnO nanocrystals [33]. In the study, morphological changes were observed with varying temperatures. Hexagonal rods were formed at 100 °C, agglomerated rods were observed at 110 °C, and flower-like structures appeared at 120 °C; it also demonstrated that varying the pH altered the various morphology, with a hexagonal structure forming at pH 7.5 and rod-like structures appearing at pH 8.5 [34]. Furthermore, reaction time also affects the formation of specific morphology of ZnO [35]. A study noted that if the reaction time was increased from 4 h to 8 h, there was a significant change from pyramid-shaped crystals (0.3 μm) to sharp lath-shaped ones. An additional 16 h led to the formation of smooth lath-like particle crystals measuring about 2 μm in diameter. Thus, long duration promotes crystal growth and improves crystallization [36]. Moreover, the pH of a solution greatly influences crystal structure. In lower pH, more nuclei form, but they grow slowly, resulting in larger nanocrystals. However, higher

Table 1
Various reaction parameters and particle properties of ZnO.

Temperature (°C)	220	200	180	160	100
Time(h)	5	6	6	6	10
Size(nm)	50–200	200–400	50–200	100–200	100–200
Morphology	Crushed stone like	Polyhedron	Sheet	Rod-like	Bullet-like

pH favors fast growth, and the synthesized crystal morphology transitions from hexagonal to flower-like [37].

In a study, spherical ZnO nanoparticles with a uniform size of approximately 7 nm were synthesized without surfactants (Fig. 3(A)). By adjusting key synthesis parameters, including reagent concentration, reaction time, and temperature, ZnO nanorods and nanoparticles were successfully obtained (Fig. 3(B)). Subsequent annealing at 900 °C for 2 h led to the formation of ZnO particles with an increased size of approximately 150 nm (Fig. 3(C)). Furthermore, a solvothermal reaction facilitated the development of hierarchical ZnO structures with a flower-like morphology and spherical shape (Fig. 3(D)). Additionally, thermal evaporation in air resulted in the synthesis of ZnO tetrapods, characterized by hexagonal legs extending from a central nucleus (Fig. 3(E)). Each distinct morphology exhibited specific structural characteristics directly influenced by the applied synthesis conditions [38].

Another study is summarized in Table 1, shows that temperature and time significantly influence the size and morphology of the synthesized crystals [39].

To synthesize the ZnO nanostructure, Hexamethylenetetramine (HMTA, $C_6H_{12}N_4$) and Zinc nitrate ($Zn(NO_3)_2$) were used as well as ($Zn(NO_3)_2$) used as the source of the Zn^{2+} ions. The weak base HMTA underwent slow decomposition, which led to an alkaline medium. This decomposition process generated the required concentration of OH^- ions for ZnO nanoparticle synthesis through the following hydrothermal reaction [33];

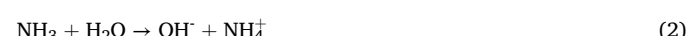


Table 2

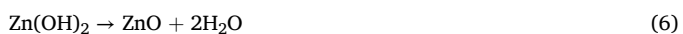
ZnO nanoparticles may be synthesized through a variety of chemical reactions.

Raw materials	Chemical reaction	Remark	Ref.
Zn(NO ₃) ₂ ·6H ₂ O, (CH ₂) ₆ N ₄	(CH ₂) ₆ N ₄ + H ₂ O → HCHO + NH ₃ H ₂ O + NH ₃ → NH ₄ ⁺ + OH ⁻ Zn ²⁺ + NH ₃ → Zn(NH ₃) ₄ ⁺ OH ⁻ + Zn(NH ₃) ₄ ²⁺ → Zn(OH) ₂ ²⁻ + NH ₃ 4OH ⁻ + Zn ²⁺ → Zn(OH) ₄ ²⁻ Zn(OH) ₂ ²⁻ → ZnO + OH ⁻ + H ₂ O	The reaction mechanism is simple and novel. Zn(OH) ₂ ²⁻ is more stable than Zn(NH ₃) ₄ ⁺ and Zn(OH) ₄ ²⁻ is formed from Zn(NH ₃) ₄ ²⁺ .	[36]
ZnCl ₂ , NaOH	ZnCl ₂ + 2NaOH → Na ⁺ + Zn(OH) ₂ ↓ + 2Cl ⁻ Zn(OH) ₂ → ZnO (hydrothermal condition; -H ₂ O)	The reaction condition is considerably moderate.	[39]
Zn(CH ₃ COO) ₂ , C ₄ H ₁₀ O ₃	Zn(CH ₃ COO) ₂ + 2H ₂ O → 2CH ₃ COOH + HO-Zn-OH Zn(OH) ₂ → 2OH ⁻ + H ₂ O + ZnO	The size of Zn(OH) ₂ was reduced as less water was supplied.	[40]



Overall synthesis methods for ZnO nanoparticles remain in equilibrium and may be adjusted by modifying reaction parameters such as temperature, precursor concentration, pH, and crystal development time. XRD spectra and spectrometers are used to examine the structure and phase composition of the resultant [33]. ZnO can be synthesized by using different raw materials (Table 2).

Additionally, ZnO was synthesized by using sodium hydroxide (NaOH), Zinc acetate dihydrate (Zn(CH₃COO)₂·2H₂O), and deionized water utilized as the solvent [41]. This process involved the following reaction;



The Raman and XRD spectra of the resultant sample suggested the existence of crystal structures and a block-like hybrid combination of Zn(OH)₂ and ZnO. Generally, flower-like ZnO was synthesized at lower temperatures (about 300 °C). UV-vis diffusion reflection spectra revealed a characteristic absorption band between 200 to 400 nm for both rod-like ZnO and the block-like ZnO/Zn(OH)₂ hybrid [41]. Table 3 records a few studies. The findings from the table demonstrate that using different reagents as the zinc source played a vital role in ZnO synthesis in either amorphous or crystalline forms. Additionally, temperature and reaction time influenced the diameter and morphology of the resulting crystals. Higher temperatures and longer reaction times resulted in crystal size and shape changes.

In summary, the hydrothermal synthesis of ZnO NMs facilitated the precise regulation of particle size, morphology, and crystallinity by adjusting various parameters such as higher pH (>10), temperature (>120 °C), and choice of zinc precursors (e.g., Zn(NO₃)₂, ZnCl₂, and Zn(CH₃COO)₂) (Fig. 4). This adaptability of ZnO NMs provides a wide range of applications, including electronics and catalysis, where particular particle attributes are essential.

1.2. Hydrothermal synthesis of CuO

Nanocrystalline CuO may be synthesized in several shapes and sizes using the hydrothermal method by modification of reaction parameters [45]. Several methods are utilized to synthesize CuO nanostructures, but hydrothermal synthesis is straightforward and environment-friendly [46]. The size and morphology of the CuO particles are directly related to their properties (e.g., catalytic activity, surface area, and electronic behavior). Therefore, controlling morphology is significant for specific

Table 3

ZnO synthesized using the hydrothermal method with various reagents in different reaction conditions, highlighting its relevant properties.

Reagent	Zn(NO ₃) ₂ ·H ₂ O, KOH, CH ₃ OH, C ₂ H ₆ O ₂	Zn(CH ₃ COO) ₂ , C ₆ H ₈ O ₇ ·H ₂ O, NaOH	(CH ₃ COO) ₂ Zn·2H ₂ O, C ₄ H ₁₀ O ₃	Zinc foils, LiOH	ZnAc ₂ ·2H ₂ O, C ₁₉ H ₄₂ BrN, KOH
Reaction temperature (°C)	120	150	160	120	120
Reaction pH	-	13	-	10	-
Morphology	Nanorods	Nanoflowers, nanorods	Rod-like	Pencil-like	Hexagonal-shaped
Amorphous/crystalline	Crystalline	Crystalline	Crystalline	Crystalline	Crystalline
Size from XRD	-	21 nm, 43 nm	6–64 nm	-	5.2069 Å, 3.2508 Å
Size from TEM (nm)	L: 100 D: 10–15	0.246, 0.245	7	D: 300 L: > 800	-
Size from SEM (nm)	L: 100 D: 10–15	100–500	-	-	L: 1400 D: 620 ± 20
Value from UV-Vis	377 nm, 392 nm	380 nm, 356 nm	380 nm	-	372 nm
Reference	[42]	[43]	[40]	[44]	[41]

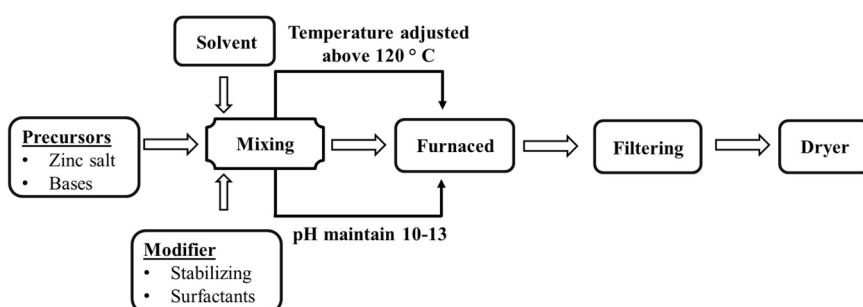
**Fig. 4.** Synthesis of ZnO using the hydrothermal method.

Table 4

ZnO nanoparticles may be generated through a variety of chemical reactions.

Raw materials	Chemical reaction	Remark	Ref.
CuSO ₄ ·5H ₂ O, NaOH, C ₆ H ₁₂ N ₄	CuSO ₄ ·5H ₂ O + NaOH → Cu(OH) ₂ + H ₂ O + Na ₂ SO ₄ Cu(OH) ₂ → CuO + H ₂ O C ₆ H ₁₂ N ₄ + H ₂ O → NH ₃ + CH ₂ O NH ₃ + H ₂ O → OH ⁻ + NH ₄ ⁺	The concentration of OH ⁻ substantially impacts the formation of CuO.	[57]
Cu (NO ₃) ₂ ·3H ₂ O, NaOH	Cu(NO ₃) ₂ ·3H ₂ O + 2NaOH → 2NaNO ₃ + Cu(OH) ₂ + 3H ₂ O 2OH ⁻ + Cu(OH) ₂ → [Cu(OH) ₄] ²⁻ [Cu(OH) ₄] ²⁻ → CuO + 2OH ⁻ + H ₂ O	The strong alkali played an important role during the synthesis method.	[58]
Cu (NO ₃) ₂ ·3H ₂ O, HNO ₃	HNO ₃ + 2Cu(OH) ₂ → H ₂ O + Cu ₂ (OH) ₃ NO ₃ 2Cu ₂ (OH) ₃ NO ₃ → 4CuO + 2NO ₂ + 3H ₂ O + 1/2O ₂ Cu ₂ (OH) ₃ NO ₃ → 2CuO + HNO ₃ + H ₂ O	In the hot liquid phase, Cu ₂ (OH) ₃ NO ₃ is generated by mixing Cu(OH) ₂ or Cu(NO ₃) ₂ with hydrochloric acid. Cu(OH) ₂ is instantaneously converted to CuO.	[59]

applications. The hydrothermal synthesis method is suitable for synthesizing CuO NPs with various shapes, such as nanosheets, nanowires, nanorods, nanoflowers, etc. [47]. This method allows precise control of reaction parameters, such as temperature, pH, duration, annealing temperature, and reactant concentration, which optimize crystal growth. These parameters significantly influence the resulting crystal's properties by changing particle size, crystallinity, and morphology [48]. Increasing hydrothermal reaction temperature and time changes the crystal structure of synthesized CuO by increasing crystal size (about 19.75–21.91 nm) [46]. Also, several studies have discussed the importance of changes in pH, additives, and annealing or calcination temperature in forming various crystal shapes. A study revealed that the resultant nanocrystal subjected to annealing at 205 °C exhibits a surface morphology similar to the original, untreated nanowires. In contrast, those annealed at 450 °C developed a rough surface along their length [49]. Predicting and controlling desirable phases and morphologies is challenging due to the lack of understanding of CuO production mechanisms under hydrothermal conditions, notably the influences of temperature, pH, and pressure. High energy requirements, variable conditions in larger reactors, and variations in precursor quality and process parameters, which result in inconsistent qualities such as crystallinity, size, and phase purity, are some of the difficulties associated with scaling up the process for industrial production [50,51]. Incorporating surfactants (e.g., CTAB), structure-directing agents, or biomimetic templates to direct the growth of nanostructures, employing in-situ characterization tools (e.g., XRD, Raman spectroscopy, and TEM) during synthesis, and utilizing microwave-assisted hydrothermal

methods for quick, consistent heating are some ways to overcome these difficulties [52,53]. Also, promising strategies for increasing efficiency and consistency include switching from batch to continuous-flow reactors, employing eco-friendly precursors, recycling byproducts, optimizing parameters with AI and machine learning, and investigating multi-element doping to produce high-entropy oxides [54].

The synthesis of CuO crystals was attempted using CuCl₂·2H₂O and C₁₈H₂₉NaO₃S. An initial homogenous solution was formed by dissolving CuCl₂·2H₂O in distilled water and continuously stirring at room temperature. Following this, C₁₈H₂₉NaO₃S dissolved into this solution again while being constantly stirred. After adding NaOH to undergo hydrothermal reactions, the resulting solution was placed inside an autoclave. This process lasted approximately 24 h under continuous heating, around 120 °C. The synthesized product was cooled to room temperature after the chemical reaction [55]. The reaction that takes place in this procedure may be enumerated as follows;



SEM image and XRD analysis were employed to characterize CuO's morphology and crystal structure. XRD analysis confirmed the formation of the monoclinic phase of CuO, indicating high purity with no detectable impurity phases. SEM imaging revealed a sheet-like morphology consistent with XRD reports. The particles were found to be approximately 0.5 μm in width and 1.2 μm in length. The synthesis occurred in a hydrothermal environment with a molar ratio of around 1:6 between Cu²⁺ and NaOH. This ratio facilitated the self-assembly of [Cu(OH)₄]²⁻ ions, resulting in the formation of 2D layered orthorhombic Cu(OH)₂ nanomaterials. TEM image further supported the sheet-like structure and revealed a porous nature with pore sizes ranging from 5 to 17 nm [55,56]. CuO may be synthesized utilizing numerous source materials (Table 4).

Additionally, CuO was synthesized through a hydrothermal method utilizing ammonia solution (NH₃·H₂O), copper (II) acetate monohydrate (Cu(CH₃COO)₂·H₂O), and sodium hydroxide (NaOH). This method was chosen for its ability to produce high-quality, pure CuO nanoparticles with controlled size and morphology. Initially, Cu(CH₃COO)₂·H₂O was dissolved into distilled water at ambient temperature with constant stirring. NH₃·H₂O solution was then added dropwise to the copper acetate solution, forming a complex. Subsequently, NaOH was introduced to precipitate copper hydroxide (Cu(OH)₂). The resulting mixture was transferred to an autoclave for hydrothermal reaction at approximately 180 °C for 24 h [60]. Ultimately, the hydrothermal synthesis of CuO is thought to occur through the following responses,

**Table 5**

Synthesis of CuO through the hydrothermal synthesis method from various sources in different reaction conditions and highlighting its relevant properties.

Reagent	Cu(NO ₃) ₂ ·2H ₂ O, NaOH	CuNO ₃ ·2.5H ₂ O, NaOH, C ₂ H ₆ O ₂	Cu(NO ₃) ₂ ·3H ₂ O, C ₂ H ₄ (NH ₂) ₂ , NaOH	CuSO ₄ ·5H ₂ O, NaOH	CuSO ₄ , NaOH
Reaction temperature (°C)	60–140	100	160	100	180
Reaction pH	11	-	-	10	8.5
Morphology	Spindle-like	Hollow sphere-like	Flake-like/sphere-like	Spherical	Flower-like
Amorphous/crystalline	Crystalline	Crystalline	Crystalline	Crystalline	Crystalline
Size from XRD (nm)	19–27	-	27.7, 12	20	18–28
Size from TEM (nm)	D: 20–40 L: 60–180 T: 30–50	-	-	-	-
Size from SEM (nm)	25, 46, 56–58	D: 29 L: 445	3.26, 5.49	-	19–28
Anneal temperature (°C)	500	-	-	200	-
Reference	[46]	[62]	[63]	[64]	[65]

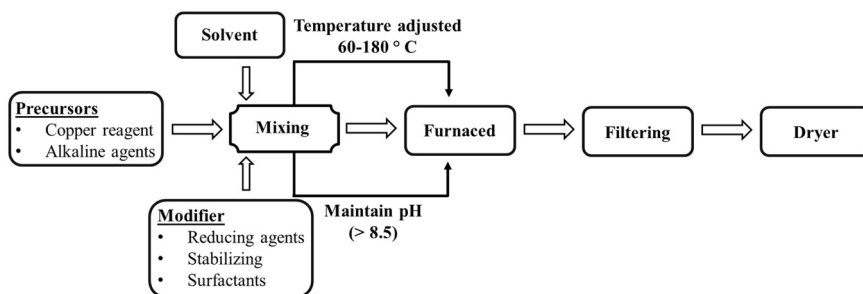
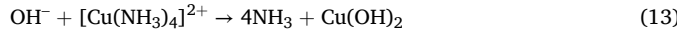


Fig. 5. Synthesis of CuO using the hydrothermal method.



The XRD analysis confirmed the successful formation of pure monoclinic CuO. This result is significant as it validates the purity of the synthesized CuO. Characteristic diffraction peaks corresponding to the desired phase were observed, while no impurity peaks, such as those from Cu(OH)₂ or Cu₂O, were detected. That result suggested that the synthesized metal oxide was pure. SEM imaging revealed a flower-like morphology for the synthesized CuO. The diameter of these flower-like structures ranged from 2 to 3 μm. This information provides insights into the size and shape control achieved in the synthesis process. TEM analysis further supported the crystallographic characteristics of the sample [60,61]. Several studies demonstrate that nanostructure CuO was synthesized by using copper (II) chloride hydrate (CuCl₂·xH₂O), copper sulfate hydrate (CuSO₄·xH₂O), copper (II) nitrate hydrate (Cu(NO₃)₂·xH₂O), copper nitrate hydrate (CuNO₃·xH₂O) as Cu sources. A few studies are recorded in Table 5. As summarized in Table 5, reaction temperature and pH strongly impact the size and morphology of the resultant CuO nanocrystal. Lower temperatures (60–200 °C) under alkaline conditions generally favor the formation of larger nanocrystals.

In summary, the hydrothermal method is highly effective for synthesizing high-quality CuO NMs with controllable properties by adjusting reaction parameters (Fig. 5). The molar ratios of copper precursors (e.g., CuCl₂, CuSO₄, Cu(NO₃)₂) to bases (e.g., NaOH) are essential in influencing the resultant CuO morphologies, including sheet-like, flower-like, and spindle-like structures. Moreover, temperature, reaction time, pH, and additives significantly affect the crystallinity, crystal dimension, and overall morphology. The adaptability of the hydrothermal method renders it a significant method for enhancing the utilization of CuO NMs in various scientific and industrial fields.

1.3. Hydrothermal synthesis of Fe₂O₃

Hydrothermal synthesis is a widely utilized method for synthesizing diverse nanostructured Fe₂O₃ with precisely regulated shapes. This method facilitates crystal growth using a high-pressure, high-temperature aqueous solution [66]. Due to their compatibility, Fe₂O₃ nanoparticles are regarded as prospective nanomaterials in the field of magnetic materials. They have been commended for their exceptional superparamagnetic properties, non-toxic nature, straightforward synthesis methods, and exceptional biocompatibility [67]. Fe₂O₃ exists in four distinct phases such as α-Fe₂O₃, β-Fe₂O₃, γ-Fe₂O₃, and ξ-Fe₂O₃. Among them, α-Fe₂O₃ has the corundum structure, but β-Fe₂O₃, γ-Fe₂O₃, and ξ-Fe₂O₃ exhibit the cubic structure [68]. Hydrothermal synthesis of Fe₂O₃ often exhibits many morphologies such as nanoparticles, micro rods, nano flakes, nano rings, nanobelts, nanofibers, nanotubes, microspheres, and hollow structures [69]. Various factors, including precursor type, solution pH, temperature, reactant concentration, and additives, may significantly influence the morphology of Fe₂O₃ nanoparticles synthesized by this method [70]. Higher concentrations often enhance nucleation rates, forming smaller particles owing to faster precursor consumption. Particle shapes and dimensions are changed by the

varying rates of degradation of different iron precursors, and the addition of surfactants may direct growth toward certain forms like rods, spheres, or plates [70,71]. In a study, Samples containing only urea or a 1:1 sodium citrate: urea ratio yielded irregularly shaped nanoparticles, not well-defined spheres. Even though some partially rounded particles were observed in the 1:1 mixture, no distinct spheres formed. This highlights the necessity of using appropriate proportions of sodium citrate and urea, as indicated by equilibrium diagrams, to achieve well-defined nanospheres [72]. Higher annealing temperatures usually lead to larger crystals by increasing development in specific directions [73]. Alongside, Various studies have also demonstrated the thermal stability of α-Fe₂O₃ nano-ellipsoids, showing that annealing temperature has minimal impact on their morphology. For instance, nano-ellipsoid morphological α-Fe₂O₃ nanocrystals with an average long-axis diameter of 275 nm and a short-axis diameter of 125 nm were synthesized by hydrothermal synthesis at 120 °C for 20 h. After annealing at 500 °C for 2 h, the size and shape remained unchanged confirming their thermal stability [74]. Furthermore, pH and surfactant impact ion stability and nucleation rates, altering the crystal growth process [70].

Traditional hydrothermal synthesis faces challenges in precisely controlling morphology (e.g., nanoparticles, nanorods) and crystal phases (α-Fe₂O₃, γ-Fe₂O₃), significantly influencing optical, magnetic, and catalytic properties. These difficulties arise from the complex interplay between synthesis parameters such as temperature, pressure, and precursor concentration. Additionally, this method requires long reaction times and high energy input and often employs toxic precursors, raising environmental concerns. To address these issues, in-situ analytical tools and machine learning can optimize and monitor real-time synthesis. Eco-friendly precursors (e.g., natural iron salts) and green solvents (e.g., water, ethanol) can replace hazardous materials. Enhancing material characteristics, improving functionality, and promoting environmental sustainability can be achieved by integrating Fe₂O₃ into hybrid systems (such as Fe₂O₃-carbon composites) during synthesis and combining hydrothermal procedures with post-treatments like calcination or plasma modification [66,75].

Fe₂O₃ has been meticulously synthesized from FeCl₃·6H₂O and NaH₂PO₄. A NaH₂PO₄ solution was carefully added drop by drop to the FeCl₃ solution while stirring continuously. The resulting solution's pH was maintained at 4.5. The mixture was then placed in a hydrothermal reactor and heated to about 240 °C for multiple hours. After the reaction, cooling the product back to room temperature was allowed. After two washes were done with distilled water and pure ethanol, and the resulting red powder was dried at 80 °C for 24 h [76]. In this experiment, Fe₂O₃ was synthesized through this method may be stated as follows,



XRD analysis identified the crystal structure of the synthesized nanoparticles and determined that crystal size decreased as the reaction

Table 6

Synthesis of Fe_2O_3 nanoparticles involves a variety of chemical reactions depending on raw materials.

Raw materials	Chemical reaction	Remark	Ref.
FeCl_3 , $\text{NH}_4\text{H}_2\text{PO}_4$	$\text{FeCl}_3 + 3\text{H}_2\text{O} \rightarrow \text{PO}_4^{3-}$ anions directly modify the shape of the crystal. Crystals turn into nanorods by increasing the aspect ratio. $\text{FeOOH} + \text{H}_2\text{O} + 3\text{HCl} \rightarrow 3\text{H}_2\text{O} + \text{Fe}^{3+}$ $2\text{Fe}^{3+} + 3\text{H}_2\text{O} \rightarrow 6\text{H}^+ + \text{Fe}_2\text{O}_3$		[78]
$\text{Fe}(\text{NO}_3)_3$, $\text{CH}_4\text{N}_2\text{O}$	$\text{CO}(\text{NH}_2)_2 + 3\text{H}_2\text{O} \rightarrow 2\text{NH}_4\text{OH} + \text{CO}_2$ $\text{NH}_4\text{OH} \rightarrow \text{OH}^- + \text{NH}_4^+$ $\text{Fe}^{3+} + 3\text{OH}^- \rightarrow \text{Fe}(\text{OH})_3 \rightarrow \text{Fe}_2\text{O}_3$	The crystallinity of the resultant Fe_2O_3 was improved over time.	[79]
$\text{FeCl}_3 \cdot 6\text{H}_2\text{O}$, $\text{C}_2\text{H}_3\text{NaO}_2$	$\text{H}_2\text{O} + \text{CH}_3\text{COO}^- \rightarrow \text{OH}^- + \text{CH}_3\text{COOH}$ $\text{OH}^- + \text{Fe}^{3+} \rightarrow \text{Fe}_2\text{O}_3 + \text{H}_2\text{O}$	The morphologies of Fe_2O_3 were highly dependent on reaction time.	[80]

time increased at 240 °C. SEM images identified irregular particle shapes with mono-metric dimensions ranging from 100 to 500 nm long and 50–160 nm wide. TEM images captured from different portions of the specimen showed size variations in the diameters of about 90–300 nm. These images also identified hollow and spindle-like structures, with hollow structures having average wall thicknesses of about 14 nm [76, 77]. Also, Fe_2O_3 can be synthesized by using different raw materials (Table 6),

Also, Fe_2O_3 was synthesized by using urea (H_2NCONH_2) and iron (III) nitrate nonahydrate ($\text{Fe}(\text{NO}_3)_3 \cdot 9\text{H}_2\text{O}$). Both precursors were separately dissolved in distilled water at room temperature. The $\text{Fe}(\text{NO}_3)_3 \cdot 9\text{H}_2\text{O}$ solution was added dropwise to the urea solution under continuous stirring. The resultant mixture was afterward stored in an autoclave and subjected to hydrothermal reaction at 140 °C for 12 h. Subsequently, the mixture was allowed to cool naturally, and the resulting sample was then filtered, rinsed, and dried in a vacuum oven at 40 °C for 6 h. Lastly, porous Fe_2O_3 microspheres were produced by

calcinating at 300 °C for 2 h [81].

XRD data demonstrated that the Fe_2O_3 microspheres that were synthesized and calcined at 300 °C made them porous and hollow. They are also pure and uniform with the Fe_2O_3 phase. SEM and TEM images identified spherical shapes, uniform sizes (about 400 nm), and porous or hollow structures. The characteristics of synthesized materials are linked to the breakdown of FeOOH . N₂-sorption analysis further demonstrated that the crystal had numerous pores (10 nm wide) and an extensive surface area (75.5 m²/g). These features increased the material's effectiveness in gas sensors with a remarkable performance in detecting ethanol gas across various concentrations and temperatures, which indicated its potential in practical applications [81]. Table 7 summarizes several related studies. The findings demonstrate that FeCl_3 and multiple salts are used as an iron source in these studies. The reaction temperature and duration affected the morphology and size of the synthesized Fe_2O_3 crystals.

In summary, the hydrothermal method is highly adaptable for obtaining controlled morphology and properties of Fe_2O_3 NMs by adjusting variables such as precursor type, reaction temperature (> 180 °C), reactant concentration, and the incorporation of additives or surfactants, which markedly influence the resulting morphologies, including nanoparticles and nanorods and hollow or porous microspheres (Fig. 6). Fe_2O_3 synthesized with this method exhibits distinct advantages, including uniformity, high purity, and enhanced surface area, making it highly suitable for various applications. In particular, porous and hollow structures demonstrate superior performance in industrial applications.

1.4. Hydrothermal synthesis of CdO

CdO NPs may be synthesized by a water-based hydrothermal method under high temperatures. CdO is an n-type semiconductor with a direct bandgap of 2.2–2.5 eV and an indirect band gap of 1.36–1.97 eV. It consists of periodic table elements from groups II and VI and is characterized by a distinctive face-centered cubic crystalline structure [88]. It also exhibits remarkable features, including having high electrical conductivity ($10^3 \text{ ohm}^{-1}\text{cm}^{-1}$) [89], significant linear refractive index

Table 7

Synthesis of Fe_2O_3 through the hydrothermal synthesis from various reagents in different reaction conditions and highlighting its relevant properties.

Reagent	$\text{FeCl}_3 \cdot 6\text{H}_2\text{O}$, NaOH , $\text{C}_2\text{H}_2\text{O}_4$	$\text{FeCl}_3 \cdot 6\text{H}_2\text{O}$, $\text{C}_6\text{H}_{14}\text{N}_2\text{O}_2$	$\text{FeCl}_3 \cdot 6\text{H}_2\text{O}$, NH_4OH , $\text{C}_2\text{H}_5\text{NO}_2$	$\text{K}_3[\text{Fe}(\text{CN})_6]$, NaOH , $\text{Na}_3\text{C}_6\text{H}_5\text{O}_7$	$\text{FeCl}_3 \cdot 6\text{H}_2\text{O}$, $\text{C}_6\text{H}_{12}\text{O}_6 \cdot \text{H}_2\text{O}$, $\text{Na}_3\text{C}_6\text{H}_5\text{O}_7 \cdot 2\text{H}_2\text{O}$	$\text{FeCl}_3 \cdot 6\text{H}_2\text{O}$, $\text{C}_2\text{H}_3\text{NaO}_2$, ($\text{C}_6\text{H}_9\text{NO}$)n
Reaction temperature (°C)	100, 120, 140, 200	180	140	180	180	200
Reaction pH	-	-	3–4	-	-	-
Morphology	Spherical Crystalline	Microspheres Crystalline	Mushroom-like Amorphous/ crystalline	Spherical Crystalline	Microspheroids Crystalline	Spherical Crystalline
Amorphous/ crystalline						
Size from XRD (nm)	21	47.04	15.3	-	27.137, 25.280	0.367
Size from TEM (460–570) nm		1.75 μm	35 nm	0.27 nm	8.32 nm, 14.65 nm	(30–40) nm
Size from SEM (300–500) nm		2 μm	5.36 μm	6.8 μm	~2.3 μm	-
Reference	[82]	[83]	[84]	[85]	[86]	[87]

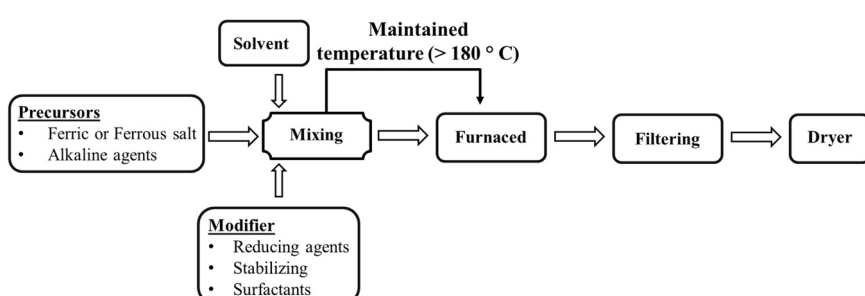


Fig. 6. Synthesis of Fe_2O_3 using the hydrothermal method.

Table 8

Synthesis of CdO nanoparticles involved different chemical reactions depending on raw materials.

Raw materials	Chemical reaction	Remark	Ref.
Cd(CH ₃ COO) ₂ ·2H ₂ O, NH ₄ OH	2NH ₄ OH + Cd(CH ₃ COO) ₂ ·2H ₂ O → 2CH ₃ COONH ₄ + Cd(OH) ₂ + 4H ₂ Cd(OH) ₂ → CdO + H ₂ O	The reaction occurred at 200 °C under a pH of 10.	[25]
Cd(NO ₃) ₂ ·2H ₂ O, H ₂ O	Cd(NO ₃) ₂ ·2H ₂ O → 4NO ₂ + O ₂ + 2H ₂ O + Cd(OH) ₂ Cd(OH) ₂ → CdO + H ₂ O	Cd(OH) ₂ is the predominant product. CdO is produced by the decomposition of Cd(OH) ₂ .	[96]

(2.49) [90], and substantial carrier mobility (142 cm²/Vs). Due to these properties, CdO is utilized in different domains, including phototransistors, solar cells, transparent electrodes, catalytic gas treatments, and chemical sensors [91]. The shape and size of synthesized CdO nanoparticles depend on reaction parameters like concentration of precursors, pressure, temperature, time of the reaction, and the addition of surfactants or other additives. These reaction parameters highly impact the crystal's nucleation, crystal growth, and aggregation [92]. High temperature and pressure usually assist in the formation of larger crystals with distinct shapes. Additionally, surfactants or additives significantly influence the morphology by encouraging specific crystal growth patterns or preventing particle agglomeration. The control of these reaction parameters enables the synthesis of various-shaped nanocrystals, including nanosheets, nanorods, nanowires, nanocubes, etc [93,94].

CdO has been synthesized from Cd(NO₃)₂ and KOH, where Cd(NO₃)₂ was used as an effective source of Cd. At first, Cd(NO₃)₂ was dissolved into the distilled water, and then the KOH solution was added gradually. The pH of the resultant mixture was maintained at a certain level. Then, the resulting mixture was placed in an autoclave bottle for 24 h for hydrothermal reaction at about 260 °C. Following the procedure, the obtained powder was rinsed with ethanol, air-dried, and then sintered at 400 °C for 2 h [95]. CdO was synthesized through this method may be stated as follows;



XRD analysis and Raman spectroscopy were utilized to analyze the synthesized CdO nanoparticles and determine their properties. The average crystallite size indicated by XRD was approximately 43 nm. SEM image revealed hexagonal nanoflake nanoparticles with an average diameter of about 150 nm. TEM analysis further confirmed that the resultant crystalline has a 100 nm edge length and thickness of about 45 nm [95]. Also, CdO may be synthesized by using different raw materials (Table 8).

Also, CdO was synthesized using cadmium nitrate tetrahydrate (Cd(NO₃)₂·4H₂O) and polyethylene Glycol (PEG). Both reactants were dissolved separately in deionized water under continuous stirring. The Cd(NO₃)₂·4H₂O solution was gradually added to the PEG solution, and the resultant solution was subsequently transferred to a hydrothermal reactor. The reactor's temperature was sustained at about 180 °C for 24 h. Finally, the consequent dried and calcined at 600 °C for 4 h [25].

XRD analysis confirmed the synthesis of CdO nanocrystals with an

average size of 28 nm. SEM images revealed uniform, aligned micro and nanosheets of CdO, assembling into spherical clusters measuring size 0.7–2 μm. Higher magnification revealed that the nanosheets, with widths of approximately 150 nm, formed face-to-face arrangements containing embedded nanoparticles. Post-treatment, the surfaces remain smooth, suggesting strong nanoparticle-nanosheet adhesion. TEM analysis also validates the sheet structure, marked by surface dots and defined edges [25]. Table 9 summarizes a few studies. The findings show that temperature, pH, and time significantly influenced the shape and size of the resulting CdO crystals.

In summer, high reaction temperatures and pressures facilitate the formation of more significant and well-defined crystals, and surfactants play a critical role in controlling morphology and preventing particle agglomeration (Fig. 7). Controlled synthesis permits the manufacture of diverse morphologies, such as nanosheets, nanorods, and spherical clusters, customized to specific purposes. Additionally, high-temperature calcination improves crystallinity and particle adherence, as demonstrated by XRD, SEM, and TEM analysis in diverse experiments.

1.5. Hydrothermal synthesis of TiO₂

The hydrothermal method was employed to synthesize TiO₂ nanoparticles in a uniform shape and size, which is straightforward and cost-effective. This method involves the chemical transformation of various titanium precursors into TiO₂ nanoparticles under high pressure and temperature. TiO₂ is a highly effective semiconductor photocatalyst with bandgap values of 3.2 eV (anatase phase), 3.02 eV (rutile phase), and 2.96 eV (brookite phase), and its absorption is predominantly observed in the UV region [99]. The resulting TiO₂ nanoparticle usually has good dispersibility, uniformity, and purity [100,101]. TiO₂ is versatile because it may exist in three distinct crystal phases: rutile, brookite, and anatase, each with its properties [102]. Reaction parameters, including temperature, time, pH, annealing temperature, and the type of precursor, can be altered to tailor the morphology of synthesized TiO₂. Changing the reaction temperature can change the resultant crystal morphology and size. For instance, a study illustrates hydrothermally synthesized TiO₂ NPs at 100 °C; shuttle-like anatase TiO₂ NPs with an average diameter of 4 nm and a length of about 23 nm were observed. As the temperature increased to 140 °C, the morphology evolved from a spherical shape with an average diameter of 9 nm to a polyhedral structure with a maximum lateral dimension of 10–30 nm at 190 °C [103]. Precursors (e.g., titanium halides, titanium sulfate, titanium alkoxides, and titanium Oxsulfate) have diverse effects on crystal formation and structural alteration. Several studies explained that

Table 9

Synthesis of CdO through the hydrothermal technique from various sources, highlighting its relevant properties.

Reagent	Cd(NO ₃) ₂ ·4H ₂ O, CH ₃ CONH ₂	Cd(NO ₃) ₂ ·6H ₂ O, NH ₄ OH	Cd(CH ₃ COO) ₂ ·2H ₂ O, NH ₄ OH	CdCl ₂ , NaOH
Reaction temperature (°C)	-	-	200	80
Reaction pH	-	8	10	-
Morphology	Cubic	Spherical	-	Rectangle shape
Amorphous/crystalline	Crystalline	Crystalline	Crystalline	Crystalline
Size from XRD (nm)	-	40.11	43	42
Size from SEM	39–41 nm	-	150 nm	43 nm
Size from TEM	41 nm	17–67 nm	100 nm	-
Calcination temperature (°C)	450	400	600	600
Reference	[97]	[92]	[98]	[89]

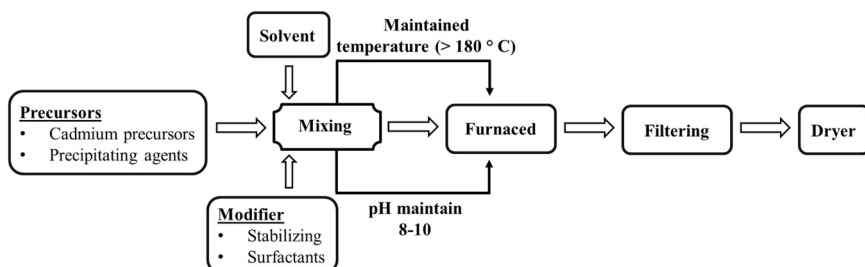


Fig. 7. Synthesis of CdO using the hydrothermal method.

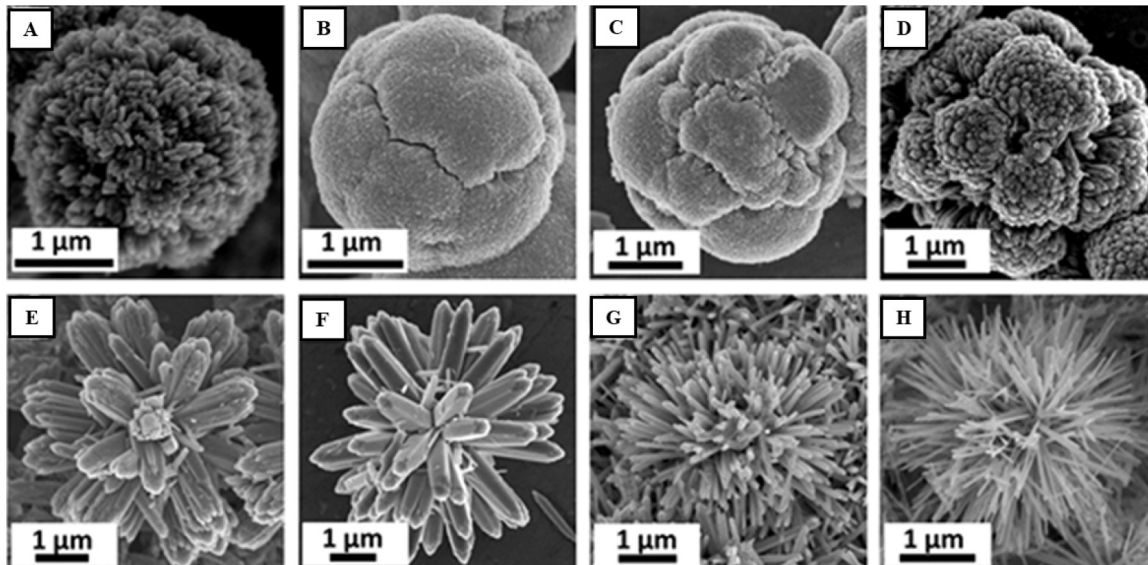


Fig. 8. FESEM images of the as-prepared 3D hierarchical rutile TiO₂ architectures, synthesized from a reaction of tetrabutyl titanate (TT) solution HCl at varying concentrations: (A) 1 M HCl, (B) 2 M HCl, (C) 3 M HCl (D) 4 M HCl (E) 5 M HCl (F) 6 M HCl (G) 7 M HCl (H) 8 M HCl [106].

strongly reactive precursors like TiCl₄ may lead to rapid crystal formation and possibly different morphologies than less reactive ones [104]. The size and crystal phase (anatase or rutile) of commercially available nanoparticle (NP) precursors may significantly alter the eventual morphology of the resulting nanostructure. Increasing the amount of precursor frequently promotes faster hydrolysis, which results in lengthy and more even TiO₂ nanorods (NRs) or any other such linear-shaped structures. A decrease in the reaction solution's pH led to the forming phase-pure rutile TiO₂ with large particle sizes. At pH levels greater than 1.09, the rutile and anatase phases are produced concurrently. According to the idea, change in pH affects both the phase transition and the development of crystals. When the pH is low, protonation can efficiently separate TiO₂ octahedra, increasing their mobility and making it easier for bigger crystallites to form by depositing individual TiO₂ octahedra onto preexisting nuclei. Conversely, a mixed phase consisting of rutile and anatase was observed at higher pH levels. The proportion of anatase increased progressively as the pH rose [105]. In a study, pH levels or precursor (HCl) concentration significantly influence resulting TiO₂ morphology. Nanorod crystals with 20 nm wide and 500 nm long (Fig. 8(A)) formed with low HCl concentration. As concentration increases, the structures transition to tennis ball-like (Fig. 8 (B-C)) formations with densely packed, radially aligned nanorods. Further increasing HCl concentration, from 2 to 5 M to 6–8 M, cauliflower-like structures (Fig. 8(E-F)) into more separated nanorod bundles due to increased etching at high HCl concentrations (Fig. 8 (G-H)) [106].

Hydrothermal synthesis of TiO₂ often requires long reaction times that consume high energy and use toxic precursors or solvents, raising

Table 10
Various reaction parameters and particle properties of TiO₂.

Volume of Ti(OBu) ₄ (ml)	3	3	0.5
Temperature(°C)	393	353	353
Morphology	Rod-like	Flower-like	Leaf-like
Phase from XRD patterns	Rutile	Rutile	Rutile
+ Anatase		+ Anatase	+ Anatase
Crystallite Size(mm) (Rutile)	14.2	6.8	11.7
Crystallite Size(mm) (Anatase)	7.0	4.5	4.5

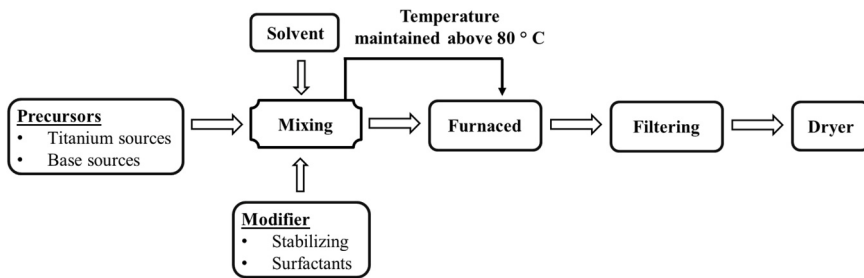
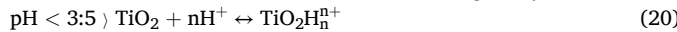
environmental and safety concerns. Bio-templates (e.g., plant extracts) or synthetic templates can be used to control morphology, and microwave-assisted heating can offer quick and energy-efficient processing to address these problems. Also, Toxicology is decreased by using environmentally friendly precursors (e.g., titanium lactate) and solvents (e.g., water or ethanol), and co-synthesis methods can enable doping (e.g., with nitrogen or sulfur), and hybridization with functional materials like carbon or metal oxides, enhancing versatility and sustainability [107]. The data in Table 10 indicates the particle properties influenced by the reaction parameters like temperature and volume of specific reagents (Ti(OBu)₄) [108].

The extended autoclaving period and greater temperature promoted the development of the crystals. A longer reaction time is likely to cause the rutile TiO₂ to agglomerate. Another study revealed that the surface acidic and essential characteristics of TiO₂ are as follows [109]:

Table 11

Synthesis of TiO₂ through the hydrothermal technique from various sources, highlighting its relevant properties.

TiO ₂ precursors	TiO ₂ powder P25 Degussa	TTIP	TBO, TiCl ₄	TiO ₂ powder P25 Degussa	TBOT	TTIP
Solvents and concentration	NaOH, 10 M	HCl	HCl	NaOH, 10 M	HCl	HCl, NaOH, HF
Reaction temperature (°C)	180	200, 180, 160, 140	80–220	175, 130	190, 175, 160, 140, 130	150
Reaction pH	2, 4, 7	-	-	-	-	-
Reaction time (h)	24	3	1–24	20, 48	3, 6	3.5
Annulation temperature (°C)	-	450	450	-	-	-
Morphology,	Nanorods, porous nanorods	Nanofibers, nanorods	Nanorods	Nanotubes, nanorods	Nanorods (130°C)	Nanorods, nanobelts, nanowires
Dimensions	L: 10 μm D: 20–200 nm	L: 1.5 μm	L: 1.9 μm D: 90 nm	L: 20–120 nm D: 20–60 nm	L: 2 μm	L: 150–250 nm
Phase (TiO ₂ NRs)	Anatase (pH=2)	Rutile	Rutile (20 h, 150 °C)	Anatase, Brookite	-	Anatase, Rutile
Reference	[112]	[113]	[114]	[115]	[116]	[117]

**Fig. 9.** Synthesis of TiO₂ using the hydrothermal method.

TiO₂ surfaces may be protonated in acidic (pH < 3.5) conditions, forming positively charged species such as TiO₂H_nⁿ⁺. On the other hand, deprotonation may take place under basic conditions (pH > 3.5), producing negatively charged species like TiO₂(OH)_nⁿ⁻. These changes in surface charge significantly influence TiO₂ NP's interactions with other materials, which impacts adsorption and photocatalysis [110].

In a study, TiO₂ was synthesized using the hydrothermal method at 180 °C, with titanium (Ti) foil as the precursor. Initially, a highly acidic solution removes impurities and oxides from titanium foil, including nitric acid (HNO₃) and hydrofluoric acid (HF). After that, deionized water and acetone rinse the foil, allowing it to dry naturally at room temperature. The purified foil fragments are placed in a hermetically sealed container with a strong NaOH alkaline solution in high-temperature and pressure situations. The process was optimized by varying temperature (130 °C to 180 °C) and duration (1 h to 12 h) to investigate the effect on the morphology of the resultants. Post-treatment at 450 °C led to the development of nanowires, nano-flowers, nanoflower, and nanofilms with increasing thickness observed at 3, 6, and 12 h, respectively.

SEM image identified the resultant crystals as nanowires with an average diameter of around 10 nm, and an XPS analysis determined the presence of titanium (Ti) and oxygen (O). Distinct peaks in the UV-visible light absorption spectra below 400 nm suggested the growth of TiO₂ crystals [111]. Table 11 summarizes findings from a few studies. It shows that the amorphous and crystalline nature of synthesized TiO₂ is highly dependent on the precursor material used. However, the morphology of the end product is highly influenced by reaction parameters such as temperature, time, pH, and annealing temperature.

In summary, the synthesis yielded a range of structures influenced by parameters such as precursor reactivity, pH, and reaction duration (Fig. 9). Reactive precursors facilitated rapid crystal growth and the formation of distinct morphologies. In contrast, precursor concentration

affected hydrolysis rates, influencing nanoparticle size and uniformity. Higher reaction temperatures and longer reaction durations promoted the formation of larger and more crystalline structures, and pH ultimately influenced interaction with other substances. Post-synthesis annealing enhanced crystallinity and phase purity, improving the material's properties for various applications.

1.6. Hydrothermal synthesis of Al₂O₃

Hydrothermal synthesis is a versatile method for synthesizing aluminum oxide (Al₂O₃) NPs by reacting aluminum precursors (like aluminum nitrate, aluminum chloride, etc.) in hot liquid media under high pressures. Al₂O₃ has different phases, including gamma (γ -Al₂O₃), eta (η -Al₂O₃), and alpha (α -Al₂O₃), etc. [118]. In reality, all other phases, including γ -Al₂O₃ and η -Al₂O₃, are metastable defect spinels, while α -Al₂O₃, also known as corundum, is thermodynamically stable. These alumina phases can undergo relatively low-energy transitions from γ -Al₂O₃ to θ -Al₂O₃ in the order $\gamma \rightarrow \delta \rightarrow \theta \rightarrow \alpha$ [119]. The phase change from γ -Al₂O₃ to α -Al₂O₃ involves changing the packing of oxygen ions from cubic to stable hexagonal close-packed structure [120]. Also, the cation additives can affect the rate of this transformation. For example, Cr³⁺, Ti⁴⁺, and Fe²⁺ accelerate it while Ba²⁺, Cs⁺, Si⁴⁺, and La³⁺ slow it down [121, 122]. To control the shape and crystal size of Al₂O₃, various parameters such as pressure, incubation time, temperature, and precursor type may be varied [123]. High temperatures (> 300 °C) may result in sintering and decreased surface area, whereas low temperatures (< 150 °C) create amorphous or weakly crystalline phases [124]. Elevated pressures stabilize crystalline phases such as γ -Al₂O₃ or α -Al₂O₃ by improving solubility and reaction kinetics. Acidic environments (pH < 7) favor denser phases like α -Al₂O₃, while extremely alkaline settings (pH > 12) favor nanostructured forms or intermediates like bayerite. The pH regulates precursor solubility and phase formation. Additives like templates or surfactants refine particle size and shape [125].

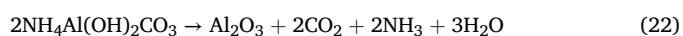
Table 12

Synthesis of Al_2O_3 nanoparticles involves different chemical reactions depending on raw materials.

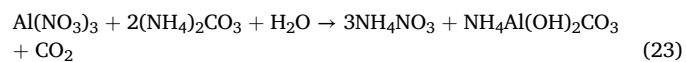
Raw materials	Chemical reaction	Remark	Ref.
$\text{Al}(\text{NO}_3)_3 \cdot 9\text{H}_2\text{O}$, H_2O	$\text{Al}(\text{NO}_3)_3 + \text{H}_2\text{O} \rightarrow \text{HNO}_3 + \text{Al}(\text{OH})_3$ $\text{Al}(\text{OH})_3 \rightarrow \text{H}_2\text{O} + \gamma\text{-AlOOH}$ $\gamma\text{-AlOOH} \rightarrow \text{H}_2\text{O} + \gamma\text{-Al}_2\text{O}_3$	$\gamma\text{-AlOOH}$ contains structural water and prevents dihydroxylation under standard conditions. However, at high temperatures, dihydroxylation of $\gamma\text{-AlOOH}$ becomes possible, leading to the formation of Al_2O_3 .	[130]
AlF_3 , $\text{C}_9\text{H}_{21}\text{O}_3\text{Al}$, $\text{C}_3\text{H}_8\text{O}$	$2\text{AlF}_3 + 3\text{H}_2\text{O} \rightarrow 6\text{HF} + \text{Al}_2\text{O}_3$ $\text{H}_2\text{O} + \text{AlF}_3 \rightarrow \text{AlOF} + 2\text{HF}$ $3\text{AlOF} \rightarrow \text{AlF}_3 + \text{Al}_2\text{O}_3$ $\text{H}_2\text{O} + 2\text{AlOF} \rightarrow 2\text{HF} + \text{Al}_2\text{O}_3$ $\text{AlF}_3 + 3\text{H}_2\text{O} \rightarrow 6\text{HF} + \text{O}_2$ $+ \text{Al}_2\text{O}$ $3\text{Al}_2\text{O} \rightarrow 4\text{Al} + \text{Al}_2\text{O}_3$ $\text{Al}_2\text{O} + 2\text{H}_2\text{O} \rightarrow 2\text{H}_2 + \text{Al}_2\text{O}_3$	Intermediate compound (AlOF) ultimately transforms into Al_2O_3	[121]

The complex interaction of synthesis parameters under the hydrothermal method makes it challenging to achieve pure phases of Al_2O_3 (such as $\alpha\text{-Al}_2\text{O}_3$ or $\gamma\text{-Al}_2\text{O}_3$, etc.) and to fine-tune their morphology. This can be solved using novel aluminum precursors such as aluminum alkoxides, bio-sourced salts, or industrial byproducts combined with inorganic or organic additives (such as templates, mineralizers, or surfactants) for precise phase and morphology control [126]. Incorporating aluminum-containing industrial waste (e.g., red mud (a byproduct of bauxite refining) and aluminum dross (from aluminum smelting) as precursors can reduce costs and environmental effects, integrating sustainability into the synthesis process [127,128]. At the same time, computational studies on the hydrothermal routes of Al_2O_3 precursors can help identify the most efficient circumstances.

Al_2O_3 nanomaterial was synthesized via the hydrothermal method using $(\text{NH}_4)_2\text{CO}_3$ and $\text{Al}(\text{NO}_3)_3 \cdot 9\text{H}_2\text{O}$, and deionized water was used as a solvent. The precursors, $(\text{NH}_4)_2\text{CO}_3$ and $\text{Al}(\text{NO}_3)_3 \cdot 9\text{H}_2\text{O}$, were mixed in an approximate molar ratio of 1:9. The mixture was then heated at 100 °C for either 24 or 36 h, followed by calcination at 800 °C for 2 h to evaluate thermal stability. About 63.0 % of weight loss is observed because of the release of bound water and decomposition of $\text{NH}_4\text{Al}(\text{OH})_2\text{CO}_3$ intermediate Al_2O_3 -hydroxide species. This process ultimately yielded Al_2O_3 nanomaterial [129].

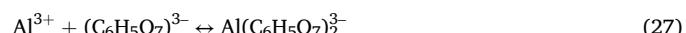
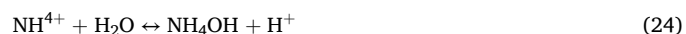


FT-IR spectroscopy confirmed that Al_2O_3 was the only component in the synthesized compounds. The peak at 3408 cm^{-1} and a weak peak at 1638 cm^{-1} indicates the presence of adsorbed water on the alumina surface due to the stretching vibrations of the OH^- group. The XRD patterns were identified as nanocrystal structures of the resultant sample. Longer hydrothermal reactions led to better crystal formation. The product contains several mesopores with a size centered at 4 nm, and the sample surface area is about 150–160 m^2g^{-1} . TEM analysis revealed uniform nanorods in the structure with lengths of 90–140 nm and 35–45 nm sizes. In contrast, the direct calcination procedure of a precipitate formed by mixing $\text{Al}(\text{NO}_3)_3 \cdot 9\text{H}_2\text{O}$ and $(\text{NH}_4)_2\text{CO}_3$ for 30 minutes at room temperature yielded irregular-shaped Al_2O_3 particles. This method ultimately generated nuclei via the following reactions,



$\text{NH}_4\text{Al}(\text{OH})_2\text{CO}_3$ decomposition yields Al_2O_3 nanorods with a high density of mesopores on their exterior surface. Subsequent calcination of the resultant liberates NH_3 , CO_2 , and H_2O [129]. Also, Al_2O_3 can be synthesized by using different raw materials (Table 12).

In another study, Al_2O_3 was synthesized through a reaction involving $\text{Al}(\text{NO}_3)_3 \cdot 9\text{H}_2\text{O}$ and $\text{C}_6\text{H}_5(\text{NH}_4)_3\text{O}_7 \cdot 2\text{H}_2\text{O}$ as precursors. Deionized water served as the solvent for this reaction. The molar ratio of Al^{3+} to citrate $(\text{C}_6\text{H}_5\text{O}_7)^{3-}$ was maintained at about 2:0 to 2:1.5. The reaction occurred by heating at 170 °C to 230 °C for 5 h, 15 h, 24 h, and 48 h, respectively. Afterward, the resultant was calcined at 550 °C for 5 h to yield the Al_2O_3 nanoparticles.



SEM image showed that the average size of the resultant particles increased gradually from 100 nm to 600 nm with increased temperatures. Additionally, the crystallinity of Al_2O_3 steadily improved with longer hydrothermal reaction times, consistent with the trend observed with increasing hydrothermal temperature. The microsphere morphology was strongly influenced by $(\text{C}_6\text{H}_5\text{O}_7)^{3-}$ concentration. If the molar ratio of Al^{3+} to $(\text{C}_6\text{H}_5\text{O}_7)^{3-}$ is 2:0, Al_2O_3 particles display irregular and inconsistent shapes. Increasing the ratio from 2:0–2:0.5, spherical Al_2O_3 gets promoted in their formations. However, further increased concentrations of $(\text{C}_6\text{H}_5\text{O}_7)^{3-}$ brought about an increase in the production of spherical particles, while too much concentration led to rod-shaped ones instead [131].

Table 13 summarizes findings from a few studies in which the

Table 13

Synthesis of Al_2O_3 through the hydrothermal technique from various sources, highlighting its relevant properties.

Reagent	$\text{Al}(\text{NO}_3)_3 \cdot 9\text{H}_2\text{O}$	H_2NCONH_2 , $\text{AlNH}_4(\text{SO}_4)_2 \cdot 12\text{H}_2\text{O}$, $\text{Na}_3\text{C}_6\text{H}_5\text{O}_7$	$\text{Al}(\text{NO}_3)_3 \cdot 9\text{H}_2\text{O}$, $\text{CO}(\text{NH}_2)_2$	$\text{Al}(\text{NO}_3)_3 \cdot 9\text{H}_2\text{O}$, $\text{C}_{10}\text{H}_{16}\text{O}_4\text{S}$	Oil shale and oil shale ash
Reaction temperature (°C)	400–500	180	160	160	160
Morphology	Spherical	Nanowires	Flower-like	Nanotubes	Flower-like (pH–13)/ leaf-like (pH–5)
Amorphous/crystalline	Crystalline	Crystalline	Crystalline	Crystalline	Crystalline
XRD generated size (nm)	-	4	21.1	-	-
TEM generated size (nm)	6	-	-	530	-
Size from SEM	-	-	L: 1–2 μm W: 10 nm, 500–800 nm	L: ~500 nm D: 20–40 nm	T: 100 nm L: 5.0–7.0 μm W: 2.0–3.5 μm
Annelation/calciation temperature (°C)	600	550	550	900	600
Reference	[130]	[132]	[133]	[134]	[135]

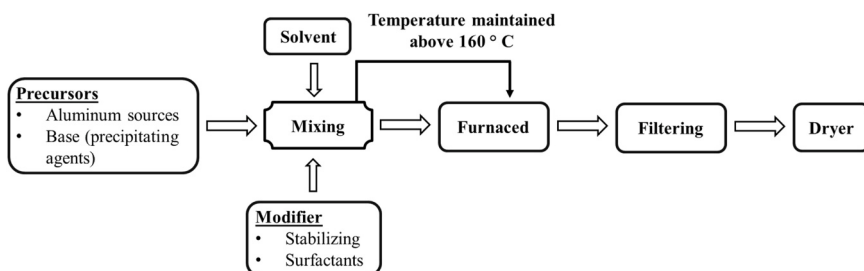


Fig. 10. Synthesis of Al_2O_3 using the hydrothermal method.

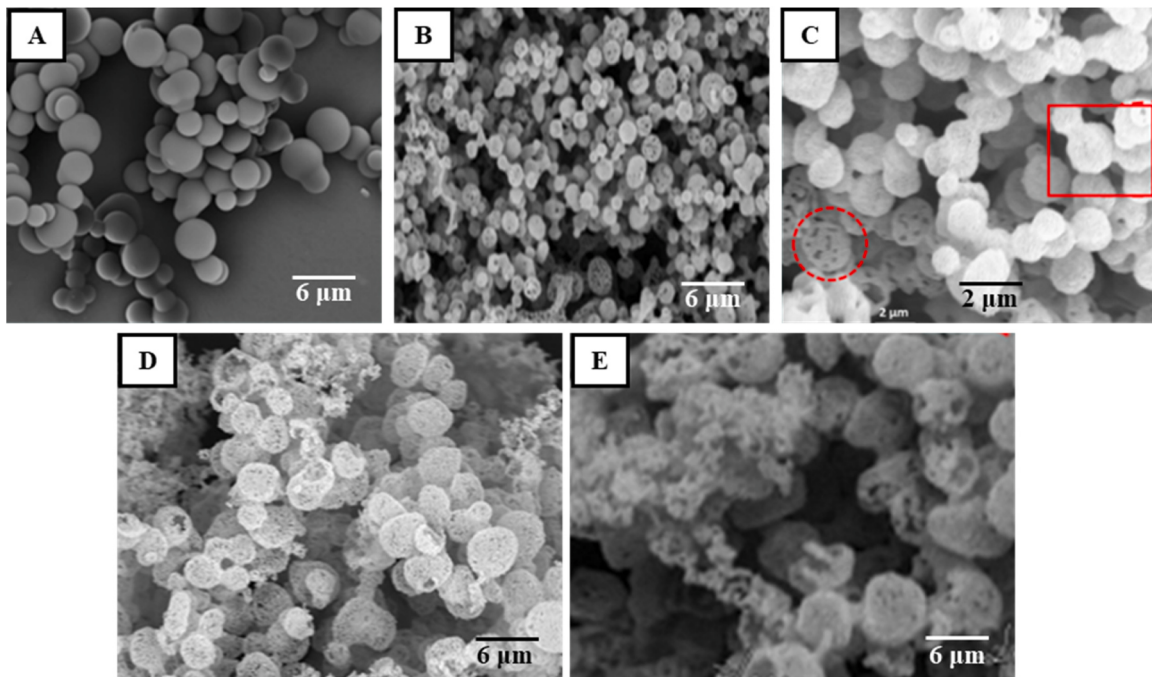


Fig. 11. SEM image CaO nanostructure hydrothermally synthesized with different reaction conditions [142].

resultant Al_2O_3 is in crystalline form. Furthermore, the shape and size of the synthesized Al_2O_3 crystals are affected by temperature, time, precursor type, and annealing temperature.

In summary, hydrothermal synthesis offers a diverse and controllable method for synthesizing Al_2O_3 NMs with tailored properties. By adjusting reaction temperature and duration, crystallinity and uniformity can be considerably enhanced (Fig. 10). Precursors such as aluminum nitrate, aluminum chloride, and ammonium aluminum carbonate hydroxide allow flexibility in reaction routes. In contrast, additional citrate reagents alter the morphology, resulting in spherical, rod-shaped, or flower-like morphologies. Additives can change phase transformation rates, crystal size, and pore structure, while the solution's pH further impacts particle shape. Finally, calcination temperatures play a key influence in defining the final phase of Al_2O_3 , with higher temperatures favoring phase stability.

1.7. Hydrothermal synthesis of CaO

The hydrothermal method synthesizes calcium oxide (CaO) through the thermally decomposing calcium-containing minerals (e.g., calcium carbonate or calcium nitrate) as well as other calcium-based minerals or compounds under certain conditions [136,137]. This method provides a cost-effective and straightforward solution-based reaction for manufacturing micro- and nanomaterials in diverse morphologies, such as nano cables, nanorods, nanostars, and nanoflowers [138]. CaO is a

multipurpose substance that exhibits outstanding catalytic, magnetic, optical, and electric properties as well as a remarkable agent for the remediation of hazardous waste and constituents in refractories and paints [139]. It facilitates alkenes to be isomerized and hydrogenated, methane to be oxidative coupled, ethane to be oxidative dehydrogenated, and H_2 (or CH_4) to be exchanged with O_2 . Also, CaO effectively absorbs SO_2 and CO_2 [140]. Reaction parameters such as type of solvent, pressure, temperature, reactant concentration, and time significantly influence the morphology of the synthesized CaO . High temperatures and pressures usually enhance the development of smaller, more uniform nanoparticles by increasing precursor solubility and accelerated nucleation. Reagent selection, surfactant, and calcination temperature are also essential. Increasing reactant concentrations often causes rapid nucleation, resulting in more oversized or irregularly shaped particles, depending on solution saturation and ionic strength [141]. In a study, disconnected spheres with limited interconnected morphology of CaO formed (Fig. 11(A)) during the initial hydrothermal treatment. Upon calcination at 800 °C, these spheres transformed into hollow, multi-shelled, highly porous structures (Fig. 11(B)). Two types of pores were observed: larger pores (circular selection) and smaller nanometric pores (square selection) (Fig. 11(C)), likely resulting from variations in the local template or metal precursor ratios during synthesis. The hollow microsphere structure remained intact (Fig. 11(D-E)) due to the porous framework, which accommodates volume changes during cycling and prevents structural damage [142].

Table 14

Synthesis of CaO nanoparticles involves different chemical reactions depending on raw materials.

Raw materials	Chemical reaction	Remark	Ref.
Ca(CH ₃ COO) ₂ •H ₂ O, C ₆ H ₁₂ O ₆	C ₆ H ₁₂ O ₆ + 6O ₂ → 6CO ₂ + 6H ₂ O Ca(CH ₃ COO) ₂ → CaCO ₃ + CH ₃ -CO- CH ₃ CaCO ₃ → CaO + CO ₂	Calcium acetate decomposes at temperatures up to 160 °C.	[148]

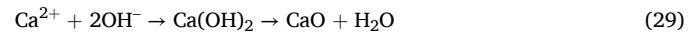
The production of byproducts, the use of dangerous solvents, and the issue of obtaining uniform CaO distribution in composites are some of the difficulties associated with scaling hydrothermal synthesis to commercial levels. These problems can be solved by developing economical synthesis pathways employing sustainable precursors, such as calcium sources generated from bio-waste (e.g., eggshells or seashells) [143]. Specific morphologies, including mesoporous CaO with high surface areas, can be guided in their growth by additives such as organic templates, structure-directing agents, or surfactants [144]. Reaction kinetics and energy efficiency are enhanced when hydrothermal synthesis is combined with techniques like ultrasonic irradiation or microwave-assisted heating. Greener substitutes for dangerous solvents, like ionic liquids or supercritical CO₂, improve sustainability and lessen their adverse environmental effects [145].

Nanostructure CaO is synthesized from CaO powder and hexadecyltrimethylammonium bromide (CTAB, C₁₆H₃₃N(CH₃)₃Br). CTAB was utilized as a surfactant. CTAB was first dissolved in deionized water, and then the CaO powder was added to the solution as a calcium source. The molar ratio of CaO to CTAB was maintained at 1:1.25. The mixed solution was subjected to ultrasonically stirring for 24 h, then placed in an autoclave for hydrothermal reaction at either 160 °C for 72 h or 240 °C for 24 h. The resultant intermediate Ca(OH)₂ was filtered, dried, and then calcined at 600 °C for 3 h to obtain single crystal porous CaO [146, 147].

The crystal structure of CaO nanoparticles was examined using XRD and SEM. XRD verified the original sample's face-centered cubic structure and intermediate compound (Ca(OH)₂). Distinct diffraction peaks were observed when the resultant CaO was calcined at 600°C without using a surfactant. SEM analysis indicated that the CaO particles had irregular morphologies and sizes ranging from 400–2000 nm. The presence or absence of surfactants during processing substantially influenced particle shape and size. Particles produced without surfactants had an irregular shape resembling a combination of the above-mentioned shapes. In contrast, surfactant-treated particles exhibited

more regular shapes like tetragonal, triangular, or hexagonal ones. In addition, the type of surfactant used significantly impacted the morphology, pore structure, surface area, and total surface area of the sample [146]. CaO can be synthesized by using different raw materials (Table 14).

In another study, CaO was synthesized by reacting Ca(NO₃)₂•9H₂O and NaOH. Initially, NaOH was dissolved in deionized water. Subsequently, a specific amount of KCl and Ca(NO₃)₂•9H₂O was mixed into the solution, and the resulting mixture was then subjected to a heat treatment at 180 °C for 12 h [149]. The discussion from Ca²⁺ ions to CaO may be stated as follows;



SEM image identified the flower-like morphology consisting of numerous cone-shaped crystals with diameters ranging from 50 to 100 nm and lengths between 0.5 and 1.0 μm. XRD analysis confirmed the predominant presence of CaO with a distinctive flower-like morphology alongside a minor amount of CaO·H₂O. The morphology of CaO was significantly affected by different NaOH concentrations, which underscored its key role in effectively synthesizing CaO. Additionally, KCl concentration played a significant role in the morphological evolution of the flower-shaped CaO structure [149, 150].

Table 15 summarizes some studies. The resultant CaO is both crystalline and amorphous, and its size and shape are affected by temperature, time, type of reagent, and annealing temperature.

In summary, the hydrothermal method is a versatile and cost-effective methodology that enables the synthesis of CaO NMs in diverse morphologies, including nanorods, nanoflowers, and nanowires. This method provides precise control over particle size and shape. High temperatures and pressures stimulated the synthesis of the smallest, more uniform NMs by enhancing solubility and accelerating nucleation. Additionally, using various surfactants, such as CTAB, and their concentrations allows for tailoring particle morphology and surface properties (Fig. 12). The choice of reagents and their ratios, exemplified by precursors like calcium nitrate or calcium carbonate, significantly influences crystallinity and particle uniformity.

2. Conclusion

This review presents the hydrothermal synthesis method for synthesizing metal oxide nanomaterials through multiple pathways, highlighting its controllability. It presents a comprehensive discussion of the hydrothermal method, highlighting the influence of reaction parameters such as temperature, reaction time, solution pH, precursor concentration, additives, and calcination temperature. The study focuses on

Table 15

CaO was synthesized using the hydrothermal method with various reagents under different reaction conditions, highlighting its relevant properties.

Reagent	Ca(CH ₃ COO) ₂ •H ₂ O, C ₆ H ₁₂ O ₆	Ca(NO ₃) ₂ •2H ₂ O, NaOH	Ca(NO ₃) ₂ •9H ₂ O, NaOH	Powder CaO, C ₁₆ H ₃₃ N(CH ₃) ₃ Br
Reaction temperature (°C)	150–200	30	180	160/240
Reaction pH	7	8.88–12.91	8–14	-
Morphology	Non-agglomerated nano powder	Nanoflower, nanorods and nanowires	Flower-like	Trigonal, tetragonal, hexagonal
Amorphous/ crystalline	Crystalline	Amorphous/crystalline	Crystalline	Crystalline
Size from XRD	92 ± 5	18.3 nm	D: 1–5 mm	400–2000 nm
Size from TEM (nm)	77	nanorods/nanowires: (~600–700) NPs: (~50–100)	0.12, 0.14, and 0.15	-
Size from SEM	-	Nanoflower (L: ~700–800 nm, D: ~300–400 nm), NPs (~50–100 nm)	L: 0.5–1.0 mm D: 50–100 nm	Trigonal (L: 90–220 nm), hexagonal (T: 60–200 nm, L: 80–400 nm), tetragonal (L: 200–750 nm, W: 50–360 nm)
Sintering Temperature (°C)	700	-	-	600
Reference	[148]	[151]	[149]	[146]

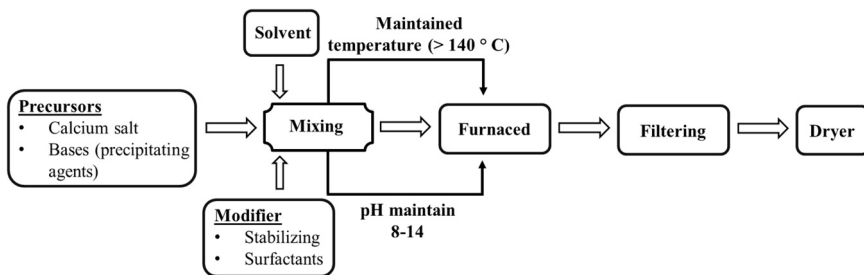


Fig. 12. Synthesis of CaO using the hydrothermal method.

different precursors for synthesizing ZnO, CuO, Fe₂O₃, CdO, TiO₂, Al₂O₃, and CaO. It examines how changes in the reaction parameters are crucial for controlling the size and morphology of the synthesized crystals. It also offers insights into choosing environmentally friendly precursors and understanding the environmental impact of by-products produced in a particular pathway. It also analyzes how hydrothermal can improve material properties by systematically modifying parameters and enhancing performance in specific applications (e.g., electronics, environmental remediation, and catalysis) through size and morphological changes. The review also underscores the importance of tailoring synthesis parameters to meet specific application requirements and compares various synthesis pathways to identify the most effective approach for particular applications.

Author Contributions

Tasnimul Quader Tazim collected the data and wrote the draft and original manuscript. Md. Kawsar assisted in collecting data and assisted in writing the manuscript. Md. Sahadat Hossain conceived and designed the review and analyzed the data. Newaz Mohammed Bahadur and Samina Ahmed supervised the findings of this work.

Declaration of Competing Interest

The authors declare that they have no known competing financial interests or personal relationships that could have appeared to influence the work reported in this paper.

Acknowledgments

The authors are grateful to the Bangladesh Council of Scientific and Industrial Research (BCSIR) authority for financial support through the R&D project (ref. no. 39.02.0000.011.14.134.2021/900; Date: 30.12.2021). Tasnimul Quader Tazim wishes to thank the Department of Applied Chemistry and Chemical Engineering, Noakhali Science and Technology University, Noakhali, Bangladesh.

Data Availability

Data will be made available on request.

References

- [1] N. Baig, I. Kammakakam, W. Falath, Nanomaterials: a review of synthesis methods, properties, recent progress, and challenges, *Mater. Adv.* 2 (6) (Mar. 2021) 1821–1871, <https://doi.org/10.1039/DOMA00807A>.
- [2] R. Bhateria, R. Singh, A review on nanotechnological application of magnetic iron oxides for heavy metal removal, *J. Water Process Eng.* 31 (Oct. 2019) 100845, <https://doi.org/10.1016/j.jwpe.2019.100845>.
- [3] T.A. Saleh, Nanomaterials: Classification, properties, and environmental toxicities, *Environ. Technol. Innov.* 20 (Nov. 2020) 101067, <https://doi.org/10.1016/j.eti.2020.101067>.
- [4] S.S. Dey, et al., Green synthesis of silver-modified bacterial cellulose with enhanced antimicrobial activity for advanced biomedical application, *Int. J. Biol. Macromol.* 307 (May 2025) 141849, <https://doi.org/10.1016/j.ijbiomac.2025.141849>.
- [5] J. Shingala, V. Shah, K. Dudhat, M. Shah, Evolution of nanomaterials in petroleum industries: application and the challenges, *J. Pet. Explor. Prod. Technol.* 10 (8) (Dec. 2020) 3993–4006, <https://doi.org/10.1007/s13202-020-00914-4>.
- [6] Y. Khan, et al., Classification, Synthetic, and Characterization Approaches to Nanoparticles, and Their Applications in Various Fields of Nanotechnology: A Review, *Catalysts* 12 (11) (Nov. 2022), <https://doi.org/10.3390/catal12111386>.
- [7] F. Wu, et al., One-step synthesis of hierarchical metal oxide nanosheet/carbon nanotube composites by chemical vapor deposition, *J. Mater. Sci.* 54 (2) (Jan. 2019) 1291–1303, <https://doi.org/10.1007/s10853-018-2889-9>.
- [8] Y. Liang, et al., Synthesis and Characterization of Fe₃O₄ Nanoparticles Prepared by Solvothermal Method, *J. Mater. Eng. Perform.* 33 (13) (Jul. 2024) 6804–6815, <https://doi.org/10.1007/s11665-023-08431-1>.
- [9] G. Asab, E.A. Zereffa, T. Abdou Seghne, Synthesis of Silica-Coated Fe₃O₄ Nanoparticles by Microemulsion Method: Characterization and Evaluation of Antimicrobial Activity, *Int. J. Biomater.* 2020 (Mar. 2020) 1–11, <https://doi.org/10.1155/2020/4783612>.
- [10] N.J. Tamanna, Md Sahadat Hossain, T.Q. Tazim, S. Tabassum, N.M. Bahadur, S. Ahmed, Utilization of marine waste for the sustainable synthesis of triple superphosphate, dicalcium phosphate, and gypsum: Exploration of crystallographic parameters using XRD data, *Clean. Waste Syst.* 10 (Mar. 2025) 100231, <https://doi.org/10.1016/j.clwas.2025.100231>.
- [11] L. Li, Y. Huang, Y. Zheng, R. Huang, J. Yao, Facile and efficient synthesis of α-Fe₂O₃ nanocrystals by glucose-assisted thermal decomposition method and its application in lithium ion batteries, *J. Power Sources* 416 (Mar. 2019) 62–71, <https://doi.org/10.1016/j.jpowsour.2019.01.080>.
- [12] A.M. Ismail, A.A. Menaze, H.A. Kabary, A.E. El-Sherbiny, A. Samy, The influence of calcination temperature on structural and antimicrobial characteristics of zinc oxide nanoparticles synthesized by Sol-Gel method, *J. Mol. Struct.* 1196 (Nov. 2019) 332–337, <https://doi.org/10.1016/j.molstruc.2019.06.084>.
- [13] M. Priya, V.K. Premkumar, P. Vasantharani, G. Sivakumar, Structural and electrochemical properties of ZnCo₂O₄ nanoparticles synthesized by hydrothermal method, *Vacuum* 167 (Sep. 2019) 307–312, <https://doi.org/10.1016/j.vacuum.2019.06.020>.
- [14] S.K. Gupta, Y. Mao, A review on molten salt synthesis of metal oxide nanomaterials: Status, opportunity, and challenge, *Prog. Mater. Sci.* 117 (Apr. 2021) 100734, <https://doi.org/10.1016/j.pmatsci.2020.100734>.
- [15] G. Yang, S.-J. Park, Conventional and Microwave Hydrothermal Synthesis and Application of Functional Materials: A Review, *Materials* 12 (7) (Jan. 2019), <https://doi.org/10.3390/ma12071177>.
- [16] M. Kawsar, M.S. Hossain, S. Tabassum, D. Islam, N. Mohammed Bahadur, S. Ahmed, Crystal structure modification of nano-hydroxyapatite using organic modifiers and hydrothermal technique, *RSC Adv.* 14 (40) (2024) 29665–29674, <https://doi.org/10.1039/D4RA0311C>.
- [17] N.K.V. Nadimpalli, R. Bandyopadhyaya, V. Runkana, Thermodynamic analysis of hydrothermal synthesis of nanoparticles, *Fluid Phase Equilibria* 456 (Jan. 2018) 33–45, <https://doi.org/10.1016/j.fluid.2017.10.002>.
- [18] A. Nandagudi, et al., Hydrothermal synthesis of transition metal oxides, transition metal oxide/carbonaceous material nanocomposites for supercapacitor applications, *Mater. Today Sustain.* 19 (Nov. 2022) 100214, <https://doi.org/10.1016/j.mtsust.2022.100214>.
- [19] S. Zhao, et al., Complex-surfactant-assisted hydrothermal synthesis of one-dimensional ZnO nanorods for high-performance ethanol gas sensor, *Sens. Actuators B: Chem.* 286 (May 2019) 501–511, <https://doi.org/10.1016/j.snb.2019.01.127>.
- [20] H. Gulab, et al., Advancements in zinc oxide nanomaterials: Synthesis, properties, and diverse applications, *Nano-Struct. Nano-Objects* 39 (Sep. 2024) 101271, <https://doi.org/10.1016/j.nanoso.2024.101271>.
- [21] S. Lettieri, M. Pavone, A. Fioravanti, L. Santamaria Amato, P. Maddalena, Charge Carrier Processes and Optical Properties in TiO₂ and TiO₂-Based Heterojunction Photocatalysts: A Review, *Materials* 14 (7) (Jan. 2021), <https://doi.org/10.3390/ma14071645>.
- [22] F. Asadzadeh, A. Poursattar Marjani, Revolutionizing acridine synthesis: novel core-shell magnetic nanoparticles and Co-Zn zeolitic imidazolate framework with 1-aza-18-crown-6-ether-Ni catalysts, *Sci. Rep.* 14 (1) (Oct. 2024) 25739, <https://doi.org/10.1038/s41598-024-75591-y>.
- [23] A. Umar, et al., Fabrication and characterization of CuO nanoplates based sensor device for ethanol gas sensing application, *Chem. Phys. Lett.* 763 (Jan. 2021) 138204, <https://doi.org/10.1016/j.cplett.2020.138204>.

- [120] S. Gramatte, et al., Atomistic Simulations of the Crystalline-to-Amorphous Transformation of γ -Al₂O₃ Nanoparticles: Delicate Interplay between Lattice Distortions, Stresses, and Space Charges, *Langmuir* 39 (18) (May 2023) 6301–6315, <https://doi.org/10.1021/acs.langmuir.2c03292>.
- [121] G. Fu, J. Wang, J. Kang, Influence of AlF₃ and hydrothermal conditions on morphologies of α -Al₂O₃, *Trans. Nonferrous Met. Soc. China* 18 (3) (Jun. 2008) 743–748, [https://doi.org/10.1016/S1003-6326\(08\)60128-4](https://doi.org/10.1016/S1003-6326(08)60128-4).
- [122] S. Shabani, S.M. Mirkazemi, H. Rezaie, Y. Vahidshad, S. Trasatti, A comparative study on the thermal stability, textural, and structural properties of mesostructured γ -Al₂O₃ granules in the presence of La, Sn, and B additives, *Ceram. Int.* 48 (5) (Mar. 2022) 6638–6648, <https://doi.org/10.1016/j.ceramint.2021.11.213>.
- [123] A.K. Eessa, A.M. El-Shamy, Review on fabrication, characterization, and applications of porous anodic aluminum oxide films with tunable pore sizes for emerging technologies, *Microelectron. Eng.* 279 (Jul. 2023) 112061, <https://doi.org/10.1016/j.mee.2023.112061>.
- [124] A.A. Khodolkova, M.V. Konyushin, A.N. Khrustalev, L.A. Arbanas, A.V. Smirnov, Y.D. Ivakin, The Direct Cold Sintering of α -Al₂O₃ Ceramics in a Pure Water Medium, *Ceramics* 7 (3) (Sep. 2024), <https://doi.org/10.3390/ceramics7030067>.
- [125] J. Sung Lee, H. Soo Kim, J. Su Lee, N.-K. Park, T. Jin Lee, M. Kang, Synthesis of α -Al₂O₃ at mild temperatures by controlling aluminum precursor, pH, and ethylenediamine chelating additive, *Ceram. Int.* 38 (8) (Dec. 2012) 6685–6691, <https://doi.org/10.1016/j.ceramint.2012.05.057>.
- [126] N. Koslowski, S. Sanctis, R.C. Hoffmann, M. Bruns, J.J. Schneider, Synthesis, dielectric properties and application in a thin film transistor device of amorphous aluminum oxide AlxOy using a molecular based precursor route, *J. Mater. Chem. C* 7 (4) (Jan. 2019) 1048–1056, <https://doi.org/10.1039/C8TC04660C>.
- [127] N. Kongkajun, B. Cherdhirunkorn, S. Kongkarat, Upcycling Mill Scale and Aluminum Dross for Sustainable Materials Processing: Synthesis of Hercynite via Fe₂O₃-Al₂O₃-C Combustion, *Recycling* 9 (5) (Oct. 2024), <https://doi.org/10.3390/recycling9050080>.
- [128] F.I.M.S. Sangor, M.A. Al-Ghouti, Waste-to-value: Synthesis of nano-aluminum oxide (nano- γ -Al₂O₃) from waste aluminum foils for efficient adsorption of methylene blue dye, *Case Stud. Chem. Environ. Eng.* 8 (Dec. 2023) 100394, <https://doi.org/10.1016/j.cscee.2023.100394>.
- [129] J. Wang, K. Shang, Y. Guo, W.-C. Li, Easy hydrothermal synthesis of external mesoporous γ -Al₂O₃ nanorods as excellent supports for Au nanoparticles in CO oxidation, *Microporous Mesoporous Mater.* 181 (Nov. 2013) 141–145, <https://doi.org/10.1016/j.micromeso.2013.07.028>.
- [130] T. Noguchi, K. Matsui, N.M. Islam, Y. Hakuta, H. Hayashi, Rapid synthesis of γ -Al₂O₃ nanoparticles in supercritical water by continuous hydrothermal flow reaction system, *J. Supercrit. Fluids* 46 (2) (Sep. 2008) 129–136, <https://doi.org/10.1016/j.supflu.2008.04.011>.
- [131] Y. Yang, et al., Hydrothermal synthesis and adsorption property of porous spherical Al₂O₃ nanoparticles, *Mater. Res. Express* 6 (7) (Apr. 2019) 075023, <https://doi.org/10.1088/2053-1591/ab1372>.
- [132] W.L. Suchanek, J.M. Garcés, Hydrothermal synthesis of novel alpha alumina nano-materials with controlled morphologies and high thermal stabilities, *CrystEngComm* 12 (10) (Sep. 2010) 2996–3002, <https://doi.org/10.1039/B927192A>.
- [133] W. Wang, J. Zhou, Z. Zhang, J. Yu, W. Cai, Different surfactants-assisted hydrothermal synthesis of hierarchical γ -Al₂O₃ and its adsorption performances for parachlorophenol, *Chem. Eng. J.* 233 (Nov. 2013) 168–175, <https://doi.org/10.1016/j.cej.2013.08.029>.
- [134] C.L. Lu, et al., Crystalline nanotubes of γ -AlOOH and γ -Al₂O₃: hydrothermal synthesis, formation mechanism and catalytic performance, *Nanotechnology* 20 (21) (May 2009) 215604, <https://doi.org/10.1088/0957-4484/20/21/215604>.
- [135] G. Ji, et al., Hydrothermal synthesis of hierarchical micron flower-like γ -AlOOH and γ -Al₂O₃ superstructures from oil shale ash, *Powder Technol.* (Jan. 2012) 54–58, <https://doi.org/10.1016/j.powtec.2011.09.005>.
- [136] W.C. Ulakpa, et al., Synthesis and Characterization of Calcium Oxide Nanoparticles (CaO NPs) from Snail Shells Using Hydrothermal Method, *JOTCSA* 11 (2) (May 2024), <https://doi.org/10.18596/jotcsa.1416214>.
- [137] S.M. Taghavi Kouzehkanan, E. Hassani, F. Feyzbar-Khalkhal-Nejad, T.-S. Oh, Calcium-Based Sorbent Carbonation at Low Temperature via Reactive Milling under CO₂, *Inorganics* 11 (5) (May 2023), <https://doi.org/10.3390/inorganics11050200>.
- [138] Maham, I. Muneer, A.N. Cheema, D. Ali, F. Yasmeen, Hydrothermal synthesis of Gd-doped CaO nanoparticles from lemon peel extract for efficient photocatalytic degradation of methylene blue under UV and sunlight, *Ceram. Int.* 50 (24) (Dec. 2024) 54064–54075, <https://doi.org/10.1016/j.ceramint.2024.10.264>.
- [139] D.K. Nguyen, V.V. On, D.M. Hoat, J.F. Rivas-Silva, G.H. Cocoletzi, Structural, electronic, magnetic and optical properties of CaO induced by oxygen incorporation effects: A first-principles study, *Phys. Lett. A* 397 (May 2021) 127241, <https://doi.org/10.1016/j.physleta.2021.127241>.
- [140] T. Hara, Y. Takami, N. Ichikuni, S. Shimazu, CaO-catalyzed Aerobic Oxidation of α -Hydroxy Ketones: Application to One-pot Synthesis of Quinoxaline Derivatives, *Chem. Lett.* 41 (5) (May 2012) 488–490, <https://doi.org/10.1246/cl.2012.488>.
- [141] K.L.A. Cao, A.M. Rahmatika, Y. Kitamoto, M.T.T. Nguyen, T. Ogi, Controllable synthesis of spherical carbon particles transition from dense to hollow structure derived from Kraft lignin, *J. Colloid Interface Sci.* 589 (May 2021) 252–263, <https://doi.org/10.1016/j.jcis.2020.12.077>.
- [142] H. Agalit, et al., Towards an agglomeration free Ca(OH)₂/CaO thermochemical energy storage loop via nanofabricated hollow CaO microspheres with highly porous shells, *Chem. Eng. J.* 493 (Aug. 2024) 152632, <https://doi.org/10.1016/j.cej.2024.152632>.
- [143] S. Piras, et al., Biomimetic Use of Food-Waste Sources of Calcium Carbonate and Phosphate for Sustainable Materials—A Review, *Materials* 17 (4) (Jan. 2024), <https://doi.org/10.3390/ma17040843>.
- [144] Y.-Q. Niu, et al., Calcium carbonate: controlled synthesis, surface functionalization, and nanostructured materials, *Chem. Soc. Rev.* 51 (18) (2022) 7883–7943, <https://doi.org/10.1039/D1CS00519G>.
- [145] C.A. Zito, M.O. Orlandi, D.P. Volanti, Accelerated microwave-assisted hydrothermal/solvothermal processing: Fundamentals, morphologies, and applications, *J. Electroceram* 40 (4) (Jun. 2018) 271–292, <https://doi.org/10.1007/s10832-018-0128-z>.
- [146] C. Liu, L. Zhang, J. Deng, Q. Mu, H. Dai, H. He, Surfactant-Aided Hydrothermal Synthesis and Carbon Dioxide Adsorption Behavior of Three-Dimensionally Mesoporous Calcium Oxide Single-Crystallites with Tri-, Tetra-, and Hexagonal Morphologies, *J. Phys. Chem. C* 112 (49) (Dec. 2008) 19248–19256, <https://doi.org/10.1021/jp8064568>.
- [147] G. Wang, et al., P123-Assisted Hydrothermal Synthesis and Characterization of Rectangular Parallelepiped and Hexagonal Prism Single-Crystalline MgO with Three-Dimensional Wormholelike Mesopores, *Inorg. Chem.* 47 (10) (May 2008) 4015–4022, <https://doi.org/10.1021/ic7015462>.
- [148] I.V. Kozerozhets, et al., A new approach to the synthesis of nanosized powder CaO and its application as precursor for the synthesis of calcium borates, *Ceram. Int.* 48 (6) (Mar. 2022) 7522–7532, <https://doi.org/10.1016/j.ceramint.2021.11.296>.
- [149] F. Liu, Y. Zhang, Hydrothermal growth of flower-like CaO for biodiesel production, *Ceram. Int.* 38 (4) (May 2012) 3473–3482, <https://doi.org/10.1016/j.ceramint.2011.12.061>.
- [150] Y. Yan, L. Zhou, Z. Han, Y. Zhang, Growth Analysis of Hierarchical ZnO Nanorod Array with Changed Diameter from the Aspect of Supersaturation Ratio, *J. Phys. Chem. C* 114 (9) (Mar. 2010) 3932–3936, <https://doi.org/10.1021/jp9122826>.
- [151] A. Samanta, et al., Synthesis of mixed calcite–calcium oxide nanojasmine flowers, *Ceram. Int.* 42 (2) (Feb. 2016) 2339–2348, <https://doi.org/10.1016/j.ceramint.2015.10.030>.